

RESEARCH ARTICLE SUMMARY

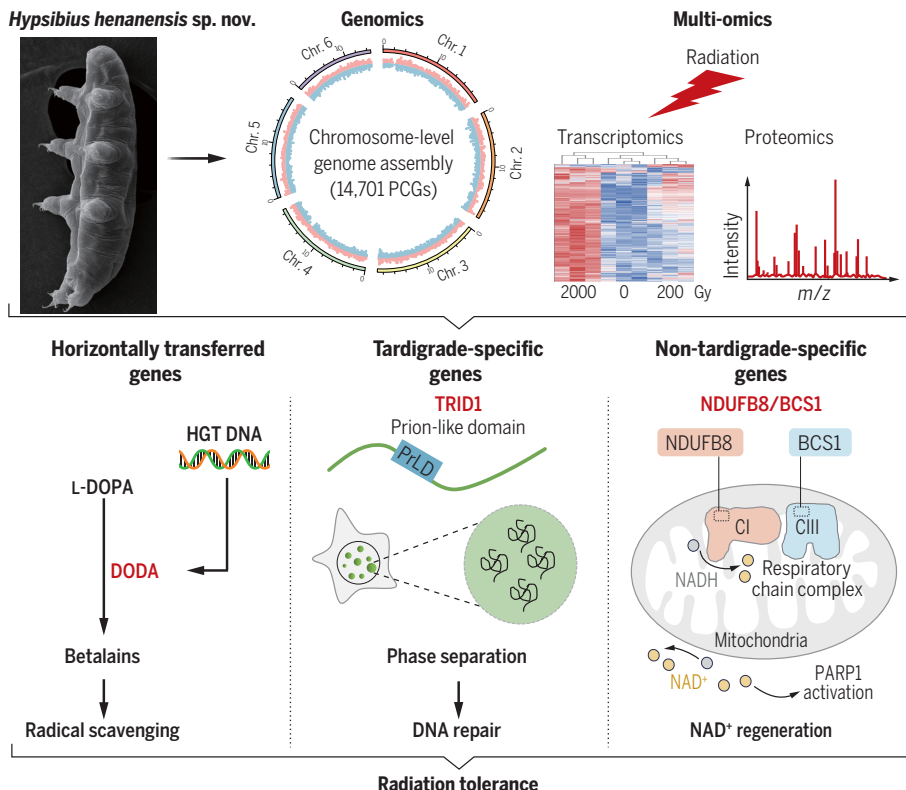
MOLECULAR BIOLOGY

Multi-omics landscape and molecular basis of radiation tolerance in a tardigrade

Lei Li (李磊)[†], Zhengping Ge (葛正平)[†], Shihao Liu (刘世豪)[†], Kun Zheng (郑坤)[†], Yaqi Li (李亚琪)[†], Kaiqi Chen (陈恺祺)[†], Yeseng Fu (付业胜)[†], Xiaoguang Lei (雷晓光), Zeling Cui (崔泽玲), Yifan Wang (王一帆), Jin Huang (黄金), Yanyan Liu (刘艳艳), Mingwang Duan (段明王), Zimei Sun (孙仔妹), Jun Chen (陈俊), Liangwei Li (李良伟), Pan Shen (沈磐), Guibin Wang (王贵宾), Junmiao Chen (陈俊苗), Ruochong Li (李若翀), Chaoran Li (李超然), Zhixiang Yang (杨志向), Yifan Ning (宁一凡), Arong Luo (罗阿蓉), Baoyu Chen (陈宝玉), Inge Seim, Xin Liu (刘心), Fei Wang (王斐), Yishan Yao (姚宜山), Fusheng Guo (郭富生), Maojun Yang (杨茂君), Cui Hua Liu (刘翠华), Guangyi Fan (范广益)*, Lizhi Wang (王立志)*, Dong Yang (杨冬)*, Lingqiang Zhang (张令强)*

INTRODUCTION: Tardigrades, commonly known as water bears, are small ecdysozoans renowned for their tolerance to extreme environments, including ultrahigh radiation. They exhibit exceptional resistance to ionizing radiation, withstanding doses as high as 3000 to 5000 grays (Gy) of gamma rays, which is ~1000 times the lethal dose for humans. The mechanism of radiotolerance in tardigrades remains largely unclear.

RATIONALE: A multi-omics data mining strategy holds immense potential for unraveling the mechanisms of extreme environmental tolerance in tardigrades. By integrating genomics, transcriptomics, and proteomics, we decipher the genome-wide landscape of antiradiation response. After differential analysis and screening of key molecules, we used biochemical and cellular methodologies to validate their functional roles and delve into the underlying molecular mechanisms.



Schematic of mechanisms that confer radiotolerance to *H. henanensis* sp. nov. The top panel shows the electron microscopy image of *H. henanensis* sp. nov. and the schematic diagram of multi-omics analysis. The bottom panel shows the three types of key radiotolerance mechanisms. The genes subjected to thorough functional and mechanistic experiments in this study are highlighted in red. PCG, protein-coding gene; m/z, mass-to-charge ratio; CI, complex I; CIII, complex III; NADH, reduced form of NAD⁺.

RESULTS: We obtained a well-annotated chromosome-level genome of a radiotolerant species, *Hypsibius henanensis* sp. nov., newly identified in this study. Through differential analysis of transcriptome and proteome after heavy ion radiation, we identified 2801 differentially expressed genes (DEGs). On the basis of evolutionary and functional analyses of these DEGs, we characterized the radiotolerance mechanisms from three different perspectives: First, horizontal gene transfer (HGT) may be an important evolutionary event that substantially contributes to the development of tardigrades' ultrahigh radiation resistance. We identified a DOPA (dihydroxyphenylalanine) dioxygenase gene, *DODA1*, that we propose is a product of HGT from bacteria to tardigrades. *DODA1* is responsive to radiation and confers radiation resistance through biosynthesis of betalains, a kind of pigment that exists mainly in plants, a few fungi, and bacteria. Next, we found that a tardigrade-specific radiation-induced disordered protein, TRID1, accelerates DNA damage repair by means of a process that encompasses phase separation. Lastly, non-tardigrade-specific genes also contribute to the tardigrades' radiotolerance. We found that two mitochondrial respiratory chain complex assembly proteins, BCS1 [ubiquinol-cytochrome c reductase (bc1) synthesis] and NDUFB8 [NADH dehydrogenase (ubiquinone) 1 beta subcomplex subunit 8], are pronouncedly up-regulated and then accumulate to accelerate NAD⁺ (nicotinamide adenine dinucleotide) regeneration for poly(adenosine diphosphate-ribosylation) (PARylation) and subsequent PARP1 [poly(adenosine diphosphate-ribose) polymerase 1]-mediated DNA damage repair.

CONCLUSION: Through multi-omics data mining and functional validation, our work uncovers a role for *DODA1* in activation of an amino acid metabolism pathway (tyrosine-DOPA-betalains axis) for reactive oxygen species mitigation, elucidates tardigrade-specific TRID1-mediated phase separation in contributing to radiotolerance by enhancing double-strand break repair efficiency, and provides insight into the participation of BCS1 and NDUFB8 in acceleration of mitochondrial oxidative phosphorylation and NAD⁺ regeneration. Functional research on these radiotolerance mechanisms of tardigrades will broaden our understanding of cell survival under extreme conditions. ■

The list of author affiliations is available in the full article online.

*Corresponding author. Email: zhanglq@nic.bmi.ac.cn (L.Z.); yangdong@ncpsb.org.cn (D.Y.); rj_wl@126.com (L.W.); fanguangyi@genomics.cn (G.F.)

†These authors contributed equally to this work.

Cite this article as L. Li et al., Science 386, eadl0799 (2024). DOI: 10.1126/science.adl0799

READ THE FULL ARTICLE AT
S <https://doi.org/10.1126/science.adl0799>

RESEARCH ARTICLE

MOLECULAR BIOLOGY

Multi-omics landscape and molecular basis of radiation tolerance in a tardigrade

Lei Li (李磊)^{1†}, Zhengping Ge (葛正平)^{1,2†}, Shihao Liu (刘世豪)^{1†}, Kun Zheng (郑坤)^{1,3*}, Yaqi Li (李亚琪)^{1†}, Kaiqi Chen (陈恺祺)^{4†}, Yesheng Fu (付业胜)^{1†}, Xiaoguang Lei (雷晓光)^{4,5}, Zeling Cui (崔泽玲)¹, Yifan Wang (王一帆)¹, Jin Huang (黄金)^{6,7}, Yanyan Liu (刘艳艳)^{1,7}, Mingwang Duan (段明王)¹, Zimei Sun (孙仔妹)¹, Jun Chen (陈俊)¹, Liangwei Li (李良伟)^{8,9}, Pan Shen (沈磐)¹, Guibin Wang (王贵宾)¹, Junmiao Chen (陈俊苗)¹⁰, Ruochong Li (李若翀)¹¹, Chaoran Li (李超然)¹, Zhixiang Yang (杨志向)¹², Yifan Ning (宁一凡)¹², Arong Luo (罗阿蓉)¹³, Baoyu Chen (陈宝玉)¹⁴, Inge Seim¹⁵, Xin Liu (刘心)⁸, Fei Wang (王斐)¹, Yishan Yao (姚宜山)¹⁶, Fusheng Guo (郭富生)⁴, Maojun Yang (杨茂君)¹¹, Cui Hua Liu (刘翠华)¹⁷, Guangyi Fan (范广益)^{8,9*}, Lizi Wang (王立志)^{14*}, Dong Yang (杨冬)^{1*}, Lingqiang Zhang (张令强)^{1*}

Tardigrades are captivating organisms known for their resilience in extreme environments, including ultra-high-dose radiation, but the underlying mechanisms of this resilience remain largely unknown. Using genome, transcriptome, and proteome analysis of *Hypsibius henanensis* sp. nov., we explored the molecular basis contributing to radiotolerance in this organism. A putatively horizontally transferred gene, DOPA dioxygenase 1 (*DODA1*), responds to radiation and confers radiotolerance by synthesizing betalains—a type of plant pigment with free radical-scavenging properties. A tardigrade-specific radiation-induced disordered protein, TRID1, facilitates DNA damage repair through a mechanism involving phase separation. Two mitochondrial respiratory chain complex assembly proteins, BCS1 and NDUFB8, accumulate to accelerate nicotinamide adenine dinucleotide (NAD⁺) regeneration for poly(adenosine diphosphate-ribosylation) (PARylation) and subsequent poly(adenosine diphosphate-ribose) polymerase 1 (PARP1)-mediated DNA damage repair. These three observations expand our understanding of mechanisms of tardigrade radiotolerance.

Tardigrades, commonly known as water bears or moss piglets, are fascinating microscopic (0.25 to 0.5 mm) invertebrates comprising the distinct phylum Tardigrada. Tardigrades have eight legs and a segmented body and inhabit diverse ecosystems (1). Approximately 1500 tardigrade species have been described (2, 3), and they have an extraordinary ability to survive in extreme conditions, including desiccation, freezing, and ionizing radiation (IR) (1, 3–5). Studies on several tardigrade species have documented that they are the most radiation-tolerant animals on Earth. They exhibit resistance to gamma radiation of up to 3000 to 5000 grays (Gy), ~1000 times higher than the lethal dose for humans (1, 6, 7). These characteristics challenge our understanding of the aqueous physiology of cells and should trouble our expecta-

tions about the limitations of biology in extreme environments.

So far, only a limited number of tardigrade genomes have been sequenced (8–11), with only one assembled genome (*Hypsibius exemplaris*) at the chromosome level, which lacks gene annotation (12, 13). With the available genome sequences, the extent of horizontal gene transfer (HGT) in tardigrades and its potential relationship with their tolerance to extreme environments have been discussed (8, 9, 11, 14), but none of these discussions involve the exploration of the radiotolerance mechanisms. Omics studies of tardigrades have primarily focused on molecular responses to desiccation (8, 9, 15–18). As for radiation tolerance, recent *in vivo* studies confirmed that tardigrades have robust DNA repair capabilities (19). Transcriptome profilings of tardigrades under gamma (19–21) and ultra-

violet (17) radiation and DNA-damaging agent treatment (21, 22) were presented. A tardigrade-exclusive protein, damage suppressor (Dsup), identified in *Ramazzottius varieornatus* (8), can confer IR resistance when expressed in human cultured cells by binding to DNA and nucleosomes and protecting DNA from radiation or hydroxyl radical damage (8, 23). Dsup also showed enhanced tolerance of radiation or oxidative damage in several different organisms and cell types (24–29). Apart from this work, much of the mechanisms underlying tardigrades' extraordinary radiotolerance remain relatively unexplored.

In this study, we leveraged our previously established tardigrade culturing system (30) to carry out morphological and molecular analysis to confirm the strain we studied, *Hypsibius henanensis* sp. nov., as a newly identified tardigrade species (see the section "Phylogeny and species delimitation of *Hypsibius henanensis* sp. nov.", figs. S1 and S2, tables S1 to S5, data S1, and movies S1 to S5). *H. henanensis* sp. nov. exhibited tolerance to desiccation and ultra-high-dose radiation (see the supplementary text in the supplementary materials and fig. S3). This species requires preconditioning (fig. S3A) to fully survive anhydrobiosis (fig. S3C). We then obtained a well-annotated chromosome-level genome of *H. henanensis* sp. nov. and carried out multi-omics profiling and functional experiments to identify critical genes that underpin the radiotolerance in *H. henanensis* sp. nov.

Results

Identification of radiotolerance-related genes

We sequenced and assembled a chromosome-level reference genome for *H. henanensis* sp. nov. Using long reads and Hi-C (high-throughput chromosome conformation capture) sequencing data, we successfully generated a high-quality genome assembly spanning 112.6 Mb and anchored to six pseudochromosomes (table S6 and figs. S4 and S5, A and B), surpassing the quality of previous tardigrade genome assemblies. Additionally, karyotype analysis confirmed that *H. henanensis* sp. nov. has a chromosome number of six (2n = 12) (fig. S5C and supplementary text). Within this reference genome, we identified 14,701 protein-coding genes that are evenly distributed across the chromosomes (fig. S5A, table S6, and data

¹State Key Laboratory of Medical Proteomics, Beijing Proteome Research Center, National Center for Protein Sciences (Beijing), Beijing Institute of Lifeomics, Beijing 102206, China. ²Department of Immunology, School of Basic Medicine, Qingdao University, Qingdao 266071, China. ³Department of Orthopedics, General Hospital of Southern Theater Command, Guangzhou 510010, China.

⁴Beijing National Laboratory for Molecular Sciences, Peking-Tsinghua Center for Life Sciences, Key Laboratory of Bioorganic Chemistry and Molecular Engineering of Ministry of Education, College of Chemistry and Molecular Engineering, Peking University, Beijing 100871, China. ⁵Institute for Cancer Research, Shenzhen Bay Laboratory, Shenzhen 518107, China. ⁶Department of Biology, Hengyang Medical School, University of South China, Hengyang 421001, China. ⁷Department of Pathophysiology, School of Basic Medicine, Anhui Medical University, Hefei 230032, China. ⁸BGI Research, Shenzhen 518083, China. ⁹BGI Research, Qingdao 266555, China. ¹⁰SCIEX China, Beijing 100015, China. ¹¹Ministry of Education Key Laboratory of Protein Science, Beijing Advanced Innovation Center for Structural Biology, Beijing Frontier Research Center for Biological Structure, School of Life Sciences, Tsinghua University, Beijing 100084, China. ¹²College of Life Science, Hebei University, Baoding 071000, China. ¹³Key Laboratory of Zoological Systematics and Evolution, Institute of Zoology, Chinese Academy of Sciences, Beijing 100101, China. ¹⁴College of Life Sciences and Food Engineering of Shaanxi Xueqian Normal University, Xi'an 710100, China. ¹⁵Marine Mammal and Marine Bioacoustics Laboratory, Institute of Deep-sea Science and Engineering, Chinese Academy of Sciences, Sanya 572006, China. ¹⁶Beijing Institute of Pharmacology and Toxicology, Beijing 100850, China. ¹⁷CAS Key Laboratory of Pathogenic Microbiology and Immunology, Institute of Microbiology, Chinese Academy of Sciences, Beijing 100101, China.

*Corresponding author. Email: zhanglq@nic.bmi.ac.cn (L.Z.); yangdong@ncpsb.org.cn (D.Y.); rj_wl@126.com (L.W.); fanguangy@genomics.cn (G.F.)

†These authors contributed equally to this work.

S2 and S3). Synteny analysis further revealed a close relationship between *H. henanensis* sp. nov. and *H. exemplaris* (fig. S6 and data S4).

To unravel the mechanisms underlying radiation tolerance in *H. henanensis* sp. nov., we exposed the tardigrades to heavy ion radiation (¹²C⁺) at the doses of 200 and 2000 Gy, followed by RNA sequencing and label-free shotgun proteomics profiling. Through this analysis, we identified 2801 differentially expressed genes (DEGs) (Fig. 1A, fig. S7, and data S5), and we examined the consistency and discrepancies between the transcriptome and proteome after irradiation (fig. S8, A and B). Most DEGs exhibited up-regulation at both the transcription and protein levels (the first quadrant in fig. S8, A and B), whereas a subset of DEGs showed up-regulation exclusively at the protein level (the fourth quadrant in fig. S8, A and B). These subsets of DEGs displayed distinct functional characteristics, with those in the first quadrant associated with DNA repair, membrane transport, and cell division, and those in the fourth quadrant primarily involved in immune response, hormone or lipid metabolism, and glycolysis (fig. S8C and supplementary text).

Comparing the DEGs among various radiation dose groups (2000 Gy versus 0 Gy and 200 Gy versus 0 Gy) revealed that many candidate genes were transcriptionally up-regulated at high versus low radiation doses (fig. S9). DEGs in the 2000 Gy group encompassed the majority of DEGs in the 200 Gy group, with 87.9% of the up-regulated genes and 76.3% of the down-regulated genes after 200 Gy radiation (fig. S9, A and B). This phenomenon was not found at the protein level (fig. S9, C and D). The shared up-regulated DEGs exhibited higher expression levels in the 2000 Gy group (fig. S9A). These shared DEGs were primarily involved in DNA repair and the assembly of mitochondrial respiratory chain (MRC) complex, whereas the DEGs exclusive to the 2000 Gy group were predominantly associated with ubiquitin-dependent protein catabolism, regulation of gene expression, and RNA processing (fig. S9E). These findings suggest that tardigrades may use a graded response mechanism to different degrees of radiation damage.

Putative horizontal gene transfer of the DOPA dioxygenase DODA1

HGT is an important driver of genome evolution in prokaryotes and is one mechanism by which recipient species adapt to extreme environments (31–33). The extent of HGT in animals, including tardigrades, has been the focus of many recent studies (11, 31, 34–36). To understand the function of HGT in this system, we identified 459 putative HGT-derived genes in the *H. henanensis* sp. nov. genome, including 75 well-supported HGT candidates (0.5% of 14,701 genes) with solid evidence (Fig. 1B, fig. S10, data S6, and supplementary text). The

proportion of HGTs in *H. henanensis* sp. nov. ranged from 0.5% to 3.1% (supplementary text), comparable to the proportions reported in other tardigrade species (8, 9, 11). Gene Ontology (GO) enrichment analysis revealed that the candidate HGT genes were associated with acetyltransferase activity, uridine diphosphate-glycosyltransferase activity, and ammonium transmembrane transport-related terms (fig. S10F).

Among the 13 up-regulated well-supported HGT genes (table S7 and data S6), the one with the highest up-regulation after irradiation (data S5) encodes a 4,5-DOPA dioxygenase called DODA1 (Fig. 1C and fig. S11), a key enzyme in the biosynthesis of betalains, a kind of pigment mainly present in Caryophyllales plants and a few bacteria and fungi (37). The functions of plant betalains are mostly related to stress resistance (37–39). In particular, the function of betalains in radiotolerance has been studied in mice (37, 40, 41). Phylogenetic analysis of this *H. henanensis* sp. nov. DODA1 (HhDODA1) was performed with currently available DOPA dioxygenase sequences from 5437 species (supplementary text and fig. S12), including 11 tardigrades with available genome (table S6) or de novo transcriptome assembly (table S8). The result revealed that HhDODA1 shared the highest sequence identity with the DODAs from the Bdellovibrionota phylum of bacteria (Fig. 1D and figs. S10 and S12).

There are five DODA genes in *H. henanensis* sp. nov. and six in *H. exemplaris* (table S9). Phylogenetic analysis shows that HhDODA1 to HhDODA4 form a distinct subfamily (figs. S12 and S13). These DODA enzymes cluster with DODAs from betalain-producing bacteria (excluding DODA from *Escherichia coli*, EcDODA, owing to its homology to plant DODAs) and fungi rather than DODAs from betalain-producing plants (fig. S13, A and B). We investigated the timing of a putative HGT event from betalain-producing bacteria. The origin of these genes likely predates the common ancestor of *H. henanensis* sp. nov. and *H. exemplaris*, with the donor gene originating from Bdellovibrionota (fig. S12). Furthermore, we predicted that HhDODA5 might have originated from a more ancient potential HGT event, occurring between a nonmetazoan organism and the ancestor of panarthropods (fig. S12). Gene expression analysis showed that, among the 21 genes in and adjacent to the *HhDODA1* loci (Chr4.1372 to Chr4.1392), only *HhDODA1* RNA expression was highly up-regulated after irradiation (Fig. 1E, table S9, and data S5).

DODA1 confers radiation resistance through betalain biosynthesis

The conversion of L-tyrosine to a secondary metabolite betalain is facilitated by the enzymes tyrosine hydroxylase and DOPA 4,5-dioxygenase (42–44) (Fig. 2A and fig. S14). To confirm the DOPA dioxygenase activity of

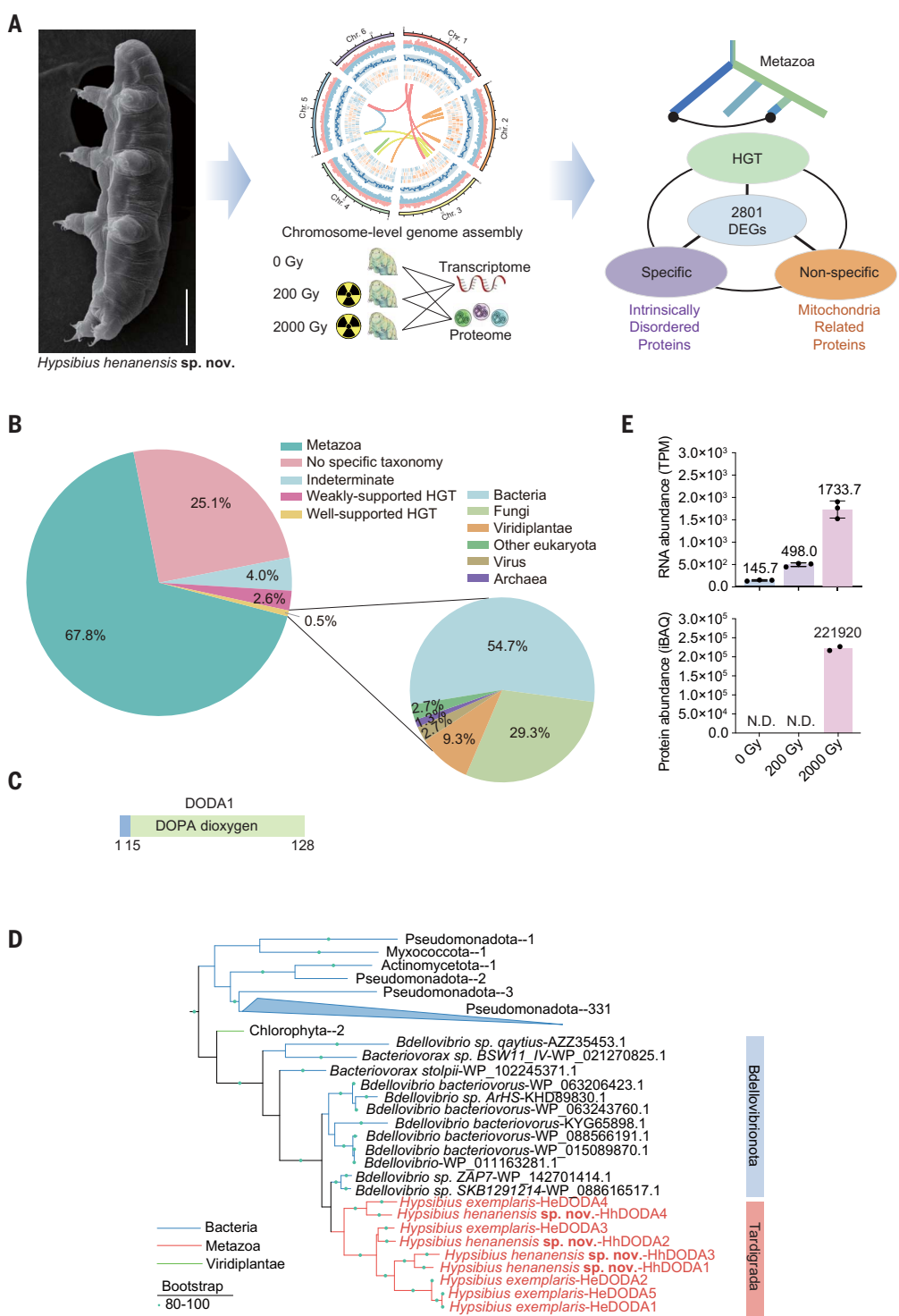
HhDODA1, both HhDODA1 and GdDODA [a well-validated DOPA 4,5-dioxygenase from the bacteria *Gluconacetobacter diazotrophicus* (45)] proteins were expressed and purified (fig. S15A), after which enzymatic assays were performed (Fig. 2B). Yellow coloring was observed in the presence of GdDODA or HhDODA1 (Fig. 2B and fig. S15B), indicating the generation of betalamic acid and dopaxanthin (45) (fig. S14). The formation of betalamic acid and dopaxanthin in GdDODA and HhDODA1 supernatants was further confirmed by ultra-performance liquid chromatography (UPLC)-ion mobility spectrometry (IMS) quadrupole time-of-flight (QTOF) (fig. S15, C to E), supporting the formation of betalamic acid from L-DOPA through the action of a 4,5-DOPA-extradiol dioxygenase enzyme (figs. S14 and S15). Betalamic acid and dopaxanthin standards were synthesized (figs. S16 and S17), and the reaction supernatant was analyzed with multiple reaction monitoring liquid chromatography-tandem mass spectroscopy (MRM-LC-MS/MS) (Fig. 2C), further confirming this process. Moreover, deuterium-labeled dopaxanthin (d₂-dopaxanthin) standards were synthesized and used for MRM-LC-MS/MS detection of the production of dopaxanthin. The results showed a coelution of dopaxanthin and d₂-dopaxanthin standard (fig. S18), indicating the production of dopaxanthin by HhDODA1.

To gain further insights into the structural basis of the dioxygenase activity of HhDODA1, we analyzed AlphaFold2-predicted structures (fig. S11) and identified putative active site residues (Fig. 2D). Alanine mutants of seven residues confirmed that five of them were involved in the catalytic activity of HhDODA1 (Fig. 2E and fig. S19, A and B). Residues H16, H18, H67, H100, and H110 of HhDODA1 are highly conserved among putative DODA proteins from *H. henanensis* sp. nov., *H. exemplaris*, and betalain-producing bacteria (except *E. coli*) and fungi, whereas E73 and D106 of HhDODA1 are less conserved (fig. S19C). A conserved motif essential for the catalytic activity of 4,5-DOPA-extradiol dioxygenases in betalain-producing plants (46) is absent in DODA proteins of *H. henanensis* sp. nov., *H. exemplaris*, bacteria, and fungi (fig. S19C).

Characterizing 4,5-DOPA-extradiol dioxygenase activity in *H. henanensis* sp. nov. led us to consider tyrosine hydroxylase to be the enzyme catalyzing the first step of betalain biosynthesis in tardigrades (Fig. 2A). Tyrosine hydroxylase genes exist in both *H. henanensis* sp. nov. and *H. exemplaris* (table S10), and their active sites are conserved from humans to tardigrades (fig. S20). Heterologous reconstitution of the betalain biosynthetic pathway in human cells was conducted by expressing HhDODA1-WT (wild type) and two mutants [His¹⁶→Ala (H16A) and D106A] in cultured human cells (HeLa) that already contained endogenous tyrosine hydroxylase (fig. S21A).

Fig. 1. Putative horizontal gene transfer of DODA.

(A) Schematic of the multi-omics profiling workflow. DEGs, differentially expressed genes; HGT, horizontal gene transfer; Specific, tardigrade-specific genes; Non-specific, non-tardigrade-specific genes. Scale bar, 50 μ m. **(B)** Classification of the gene repertoire of *H. hananensis* sp. nov., according to their putative taxonomic origins and compositions of candidate HGT genes. **(C)** The *H. hananensis*. Chr4.1382 encoded 128-amino acid DODA1 is represented, the DOPA dioxygen domain (green) is shown. **(D)** Subtree from maximum likelihood phylogenetic analysis of the horizontally transferred gene *HhDODA1*-4. Bootstrap support is indicated on the branches. The triangle shape represents the collapsed subtree containing at least three phyla, and the phylum occupying >90% sequences in the subtree is shown. The values after the phylum names are the number of sequences included in the tree. The complete results are presented in fig. S12. For accession numbers and the raw tree file, see data S10. **(E)** RNA and protein abundance of *HhDODA1* from transcriptome and proteome data, respectively. The data are presented as mean \pm SD ($n = 3$ replicates). iBAQ, intensity-based absolute quantification; TPM, transcripts per million; N.D., not detected.



Standards of betaxanthins and betalamic acid were synthesized (figs. S16 and S17) and used for MRM-LC-MS/MS detection of the production of betalains from the extracts of HeLa cells expressing DODA1 (table S11). The results showed that betalamic acid, phenylalanine-betaxanthin, valine-betaxanthin, and proline-betaxanthin were detected both in DODA1-WT and DODA1-D106A-expressing HeLa cells, but

not in DODA1-H16A (where the active site was abolished), RvDsup-expressing HeLa cells and control cells (Fig. 2F and figs. S21B and S22). These results confirmed the successful establishment of the betalain biosynthetic pathway in human cells and the involvement of HhDODA1 as a DOPA dioxygenase in betalain biosynthesis.

To evaluate the radioprotective effect of HhDODA1, along with the complete betalain

synthesis pathway in cultured human cells, we used three different techniques. Colony formation assays demonstrated that HhDODA1-WT had an obvious radioprotective effect comparable to the positive control RvDsup (Fig. 2G and fig. S23A). Additionally, alkaline comet assays showed that HhDODA1-WT and HhDODA1-D106A reduced irradiation-induced DNA fragmentation, whereas HhDODA1-H16A failed to

Fig. 2. HhDODA1 confers radiation resistance by betalain biosynthesis.

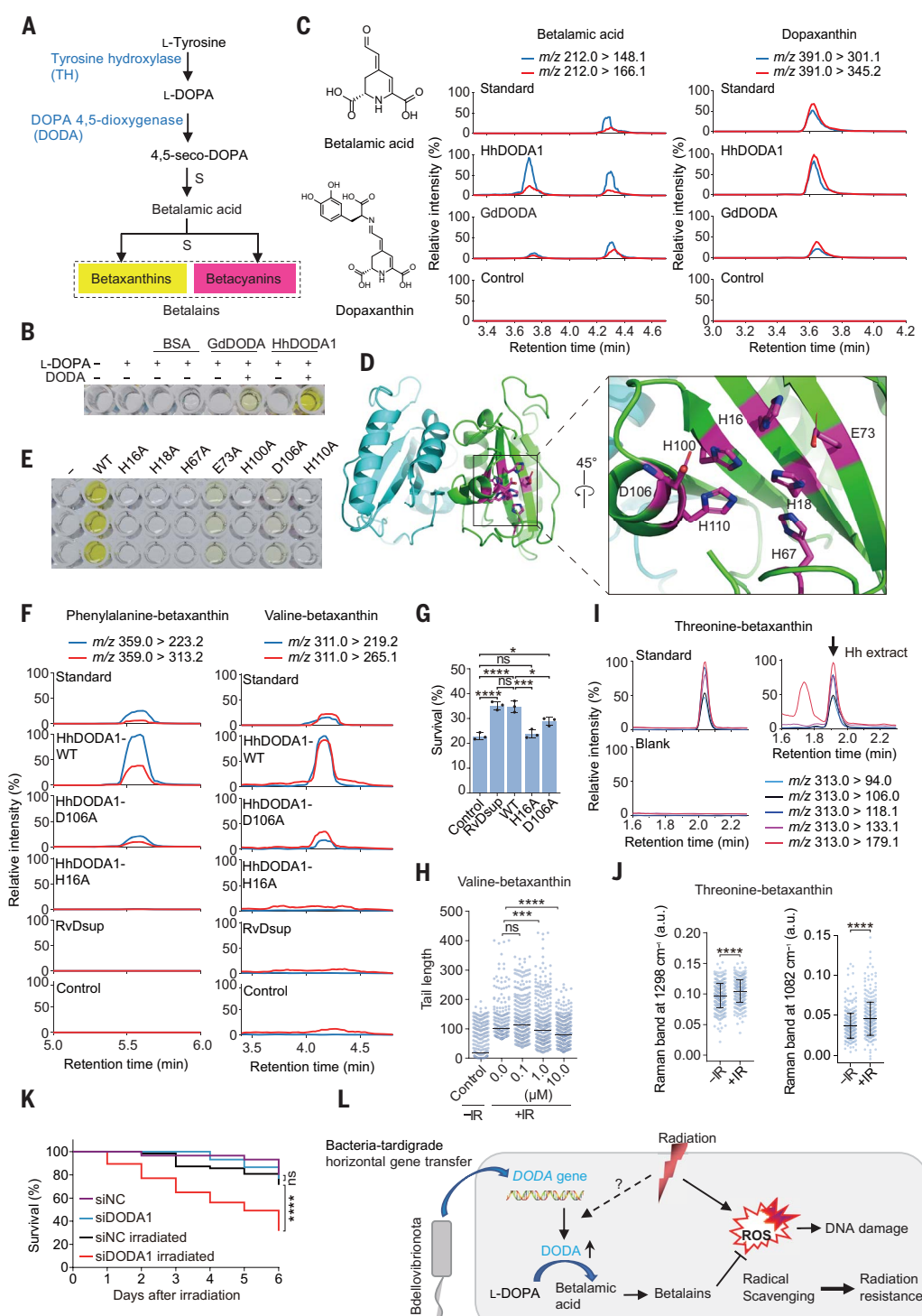
(A) Simplified biosynthetic scheme of betalains from L-tyrosine catalyzed by tyrosine hydroxylase and DODA. Detailed biosynthetic pathway is shown in fig. S14. S, spontaneous.

(B) Enzyme activity assay of GdDODA (0.375 µg/µl) or HhDODA1 (0.04 µg/µl) supplemented with 2.5 mM L-DOPA in 50 mM sodium phosphate (pH 7.0). BSA, bovine serum albumin. (C) MRM-LC-MS/MS identification of betalamic acid and dopaxanthin from the HhDODA1 or GdDODA reaction supernatant in the presence of L-DOPA by using betalamic acid and dopaxanthin standards.

Structures of betalamic acid and dopaxanthin and representative MRM-LC-MS/MS chromatograms of betalamic acid, [M+H]⁺ m/z (mass-to-charge ratio) 212.0 > 148.1 and m/z 212.0 > 166.1, and dopaxanthin, [M+H]⁺ m/z 391.0 > 301.1 and m/z 391.0 > 345.2, are shown. (D) Potential functional residues (magenta) in a AlphaFold2 predicted model of HhDODA1. The two subunits of HhDODA1 dimer are shown in green and cyan, respectively. Single-letter abbreviations for the amino acid residues are as follows: A, Ala; D, Asp; E, Glu; H, His.

(E) Production of betalains in samples of HhDODA1-WT or mutant proteins supplemented with L-DOPA. (F) Representative MRM-LC-MS/MS chromatograms of phenylalanine-betaxanthin, [M+H]⁺ m/z 359.0 > 223.2 and m/z 359.0 > 313.2, and valine-betaxanthin, [M+H]⁺ m/z 311.0 > 219.2 and m/z 311.0 > 265.1, in the extracts of HeLa cells expressing the indicated proteins. The complete results are presented in fig. S21B. (G)

HeLa cells stably expressing indicated proteins were treated with or without 5 Gy IR, and the cell survival rates were counted by colony formation assay. The data are presented as mean ± SD ($n = 3$ replicates). (H) The effects of different dose of valine-betaxanthin on protection of HeLa cells from DNA damage under nonirradiation or 10 Gy x-ray irradiation condition in alkaline comet assays. DNA fragmentation was assessed by the tail length. At least 266 cells were analyzed for each condition. The median values are shown as a black bar. The unit of tail length is µm. (I) Targeted mass spectrometry analysis of the extract of *H. henanensis* sp. nov. (Hh extract) by MRM-LC-MS/MS. Representative MRM-LC-MS/MS chromatograms of threonine-betaxanthin standard, the Hh extract, and the blank are shown. The black arrow indicates the peak of threonine-betaxanthin identified in the Hh extract. The detailed information of the daughter ions is presented in fig. S24B. (J) Semiquantification of threonine-betaxanthin by their Raman band intensities at 1298 cm⁻¹ and 1082 cm⁻¹ from living *H. henanensis* sp. nov. specimens 2 days after 500 Gy IR treatment. Three hundred eighty-one single spectra from nine specimens without IR and 354 single spectra from 14 specimens with 500 Gy IR were analyzed. The data are presented as mean ± SD. a.u., arbitrary units. (K) The survival rate of control and DODA1 siRNA-soaked tardigrades with or without 500 Gy IR. At least 30 individuals were analyzed for each condition. (L) A proposed model that a putative horizontally transferred DOPA dioxygenase gene *HhDODA1* from bacteria is responsive to radiation and involved in betalains biosynthesis, which confers radiotolerance. One-way analysis of variance (ANOVA) with Tukey's post hoc test for (G). Kruskal-Wallis test followed by Dunn's test for (H). Mann-Whitney U test for (J). Simple survival analysis (Kaplan-Meier) with log-rank test for (K). P > 0.05, not significant (ns); *P < 0.05; **P < 0.001; ***P < 0.0001.



alleviate DNA fragmentation (fig. S23, B and C). DNA double-strand breaks (DSBs) are particularly harmful (47), and we further assessed the impact of HhDODA1 on genome integrity maintenance and DSB repair using the DSB indicator γ H2AX. Cells expressing HhDODA1-WT and HhDODA1-D106A exhibited fewer γ H2AX foci compared with control cells (fig. S23, D and E). In addition, expression of HhDODA1-WT and its mutants did not affect cell cycle distribution (fig. S23F), indicating that the improved radiotolerance by HhDODA1 was not due to cell cycle alterations.

IR exerts its biological effects through two mechanisms: direct action and indirect action. The latter, mediated by reactive oxygen species (ROS), accounts for 60 to 70% of the effects of IR (48, 49). Previous studies have highlighted the antioxidant and free radical-scavenging activities of betalains (37, 43, 50–52). On the basis of this knowledge, we hypothesized that betalains synthesized by HhDODA1 might contribute to radiation resistance by scavenging radicals. Analysis of ROS levels in irradiated HeLa cells revealed a drastic decrease in HhDODA1-WT-expressing cells and a moderate decrease in HhDODA1-D106A cells, whereas HhDODA1-H16A showed no difference compared with the control cells (fig. S23, G to I). Moreover, different concentrations of three betaxanthins identified in DODA1-expressing HeLa cells (Fig. 2F and fig. S21B) were used to perform comet assay to assess the radioprotective effect. The results showed that 1 μ M of these three betaxanthins had a significant radioprotective effect. As the concentration increased, the protective effect became stronger (Fig. 2H and fig. S23J).

Given the above data, we expected that DODA1 could also produce betalains and confer radiation resistance through betalain biosynthesis in *H. henanensis* sp. nov. Using untargeted mass spectrometry analysis, we found that four candidate betalains were identified in the extract of *H. henanensis* sp. nov. (fig. S24A). Standards of betaxanthins and betalamic acid (figs. S16, S17, and S22) were synthesized and further used for targeted mass spectrometry analysis of the extract of *H. henanensis* sp. nov. by MRM-LC-MS/MS (table S12). Threonine-betaxanthin was identified in the extract of *H. henanensis* sp. nov. (Fig. 2I and fig. S24, B and C). Raman spectroscopy also revealed that, in the control group, threonine-betaxanthin was concentrated on the pharyngeal bulb and the second and the third claws of *H. henanensis* sp. nov. In the IR-treated group, threonine-betaxanthin was evenly distributed on the surface of the body and the placoid body (fig. S25, A and B). Quantitative analysis showed that threonine-betaxanthin in *H. henanensis* sp. nov. was up-regulated in response to IR (Fig. 2J and fig. S25B), which is consistent with the results that HhDODA1 RNA expression

was highly up-regulated after radiation (Fig. 1E). As determined by small interfering RNA (siRNA) soaking methods developed by us (fig. S25C), endogenous DODA1 was knocked down in tardigrades (fig. S25D). Raman spectroscopy analysis showed that, after DODA1 knockdown, threonine-betaxanthin in *H. henanensis* sp. nov. was down-regulated (fig. S25E). DODA1 knockdown decreased the survival rate of tardigrades 6 days after irradiation (Fig. 2K), confirming the in vivo radioprotective effect of DODA1. Collectively, these findings indicated that HhDODA1, functioning as a DOPA dioxygenase involved in betalain biosynthesis, confers radiotolerance (Fig. 2L).

The tardigrade-specific radiation-induced disordered protein TRID1 promotes DSB repair through phase separation

By investigating homologous genes across the three superkingdoms, we categorized a total of 14,701 genes in the *H. henanensis* sp. nov. genome into four groups: genes common in cellular organisms (I_Ce), genes common in Eukaryota (II_Eu), genes common in Metazoa (III_Me), and genes specific to Tardigrada (IV_Tar) (Fig. 3A). We defined 4436 tardigrade-specific genes, accounting for 30.2% of the total genes. Using weighted gene coexpression network analysis, we identified a subset of tardigrade-specific genes within the “2000 Gy up-regulated module” that are potentially involved in DNA repair, nucleic acid metabolism, cell cycle, and proteolysis (fig. S26 and supplementary text). In addition to expression and functional analysis, we considered structural disorder characteristics of the proteins because intrinsically disordered proteins have long been known to help mediate tolerance to different abiotic stresses including desiccation, osmotic stress, high temperatures, and freezing in diverse organisms (18, 53–61). Many tardigrade-specific proteins have sequence features indicating intrinsic disorder (Fig. 3B). More importantly, among the proteins encoded by tardigrade-specific radiation-induced up-regulated genes, 39.1% (163/417) were highly disordered, a proportion significantly higher than that observed for the genes common in cellular organisms (I_Ce, 7.2%, 45/626) (Fig. 3B). These results suggest the tardigrade-specific disordered proteins may be related to radiation response or tolerance.

In the above analysis of the radiation-induced up-regulated proteins with predicted disorder (fig. S27A), we discovered a protein referred to as tardigrade-specific radiation-induced disordered protein 1 (TRID1), because of its intrinsic disorder score and nuclear localization signal sequence. TRID1 features a prion-like domain (PrLD) (Fig. 3C), which is a type of low-complexity domain rich in uncharged polar amino acids and has a propensity to self-assemble and form aggregates (62). To investigate whether

TRID1 might undergo phase separation on its own, we expressed and purified green fluorescent protein (GFP)-tagged TRID1 (GFP-TRID1) (fig. S27B) for phase separation assays. In a buffer containing 50 mM NaCl, TRID1 formed droplets (Fig. 3D). However, as the NaCl concentration increased, the number and size of droplets decreased, and droplet formation was completely abolished at 300 mM NaCl (Fig. 3D). Furthermore, the GFP-TRID1 droplets exhibited fusion, indicating droplet coalescence (Fig. 3E). Fluorescence recovery after photobleaching (FRAP) analysis demonstrated the rapid redistribution of GFP-TRID1 from the unbleached area to the bleached area (Fig. 3F). To investigate the role of the PrLD domain in the phase separation of TRID1, we generated a GFP-tagged PrLD deletion (Δ PrLD) mutant (Fig. 3G and fig. S27B) and examined its droplet formation in vitro. Unlike TRID1-WT, the TRID1- Δ PrLD mutant formed protein aggregations instead of droplets in 50 mM NaCl (Fig. 3H). However, when the concentration of NaCl increased to 150 mM, TRID1- Δ PrLD could also form droplets, although in fewer numbers and smaller sizes compared with TRID1-WT droplets (Fig. 3H). Furthermore, we added 1,6-hexanediol, a chemical commonly used to disrupt phase-separated condensates, to confirm the liquid-like nature of the droplets. Both TRID1-WT and TRID1- Δ PrLD droplets disappeared upon the addition of 1,6-hexanediol (fig. S27C). To investigate whether TRID1 undergoes liquid-liquid phase separation (LLPS) in a cellular context, we ectopically expressed GFP-TRID1-WT and GFP-TRID1- Δ PrLD in HeLa cells (fig. S27D). GFP-TRID1-WT formed droplets within the nucleus of HeLa cells (Fig. 3I). FRAP analysis further demonstrated the dynamic nature of droplets formed by GFP-TRID1-WT (fig. S27E). In comparison, GFP-TRID1- Δ PrLD formed small punctum structures in the nucleus of cells. Both the droplets formed by TRID1-WT and the punctum structures formed by TRID1- Δ PrLD were sensitive to treatment with 1,6-hexanediol (Fig. 3I), indicating that the PrLD was crucial for the droplet formation.

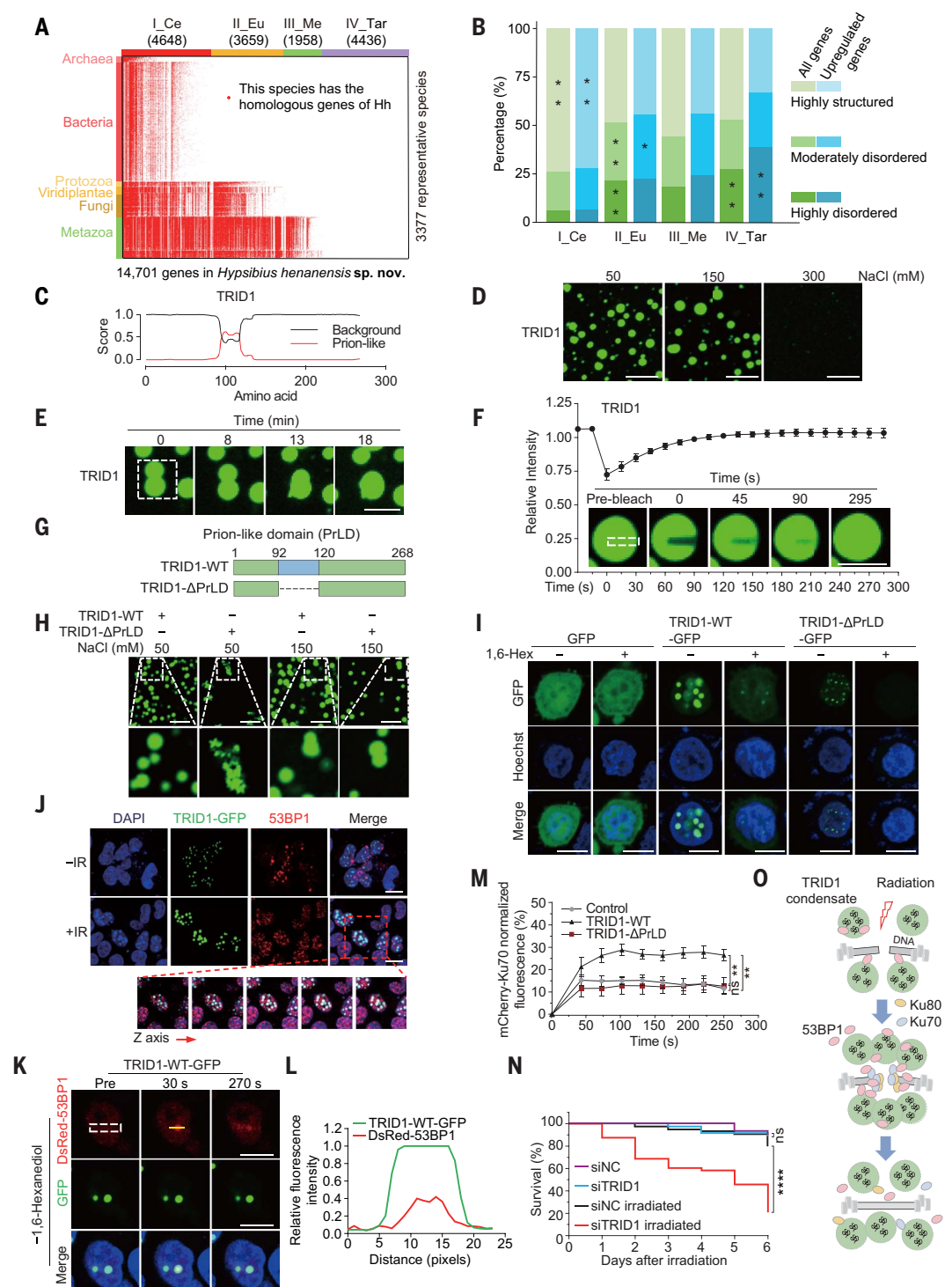
Considering that TRID1 was up-regulated upon exposure to radiation, we hypothesized that TRID1-mediated LLPS confers radioprotective effects. Colony formation and immunofluorescence assays were conducted using U2OS cells to assess the impact of TRID1 on cell survival after radiation exposure. TRID1-WT, as well as the positive control RvDsup, exhibited a radioprotective effect, whereas TRID1- Δ PrLD had no effect (fig. S27, F to H, and movie S6). To further investigate whether the radioprotective effect of TRID1 could be attributed to enhanced DSB repair, we examined the effect of TRID1 on the repair efficiency of the major DSB repair pathways, namely nonhomologous end joining (NHEJ) and homologous recombination (HR), using EJ5-GFP and DR-GFP

Fig. 3. Tardigrade-specific protein TRID1-mediated liquid-liquid phase separation has radioprotective effects by enhancing recruitment of DNA repair proteins to DSB sites.

(A) Homologous gene distribution of 14,701 genes of *H. henanensis* sp. nov. (Hh) in 3377 species (including Hh itself) across the three superkingdoms, and classification of the four evolutionary age grades (I_Ce, cellular organism; II_Eu, Eukaryota; III_Me, Metazoa; IV_Tar, Tardigrada). Each column represents one of the 14,701 genes, and each row represents one of the 3377 species. (B) Proportion distribution of disorder levels of the protein product of all Hh genes or the up-regulated genes in four evolutionary age grades [the same as (A)]. * and ** represent $P < 0.05$ and $P < 1 \times 10^{-10}$, respectively, for the over-representation analysis.

(C) Prediction of prion-like domain (PrLD, denoted by the red line) in TRID1 by using Prion-Like Amino Acid Composition (PLAAC) (<http://plaac.wi.mit.edu/>). (D) Phase separation of TRID1 (10 μ M) with increasing concentrations of NaCl in the phase separation buffer (50 mM Tris-HCl, 1 mM EDTA, 1 mM dithiothreitol, 50 to 300 mM NaCl, pH 7.5). (E) Fusion of TRID1 (10 μ M) droplets in 150 mM NaCl.

(F) Fluorescence intensity of TRID1 droplets after photobleaching were plotted over time. Representative images of fluorescence recovery are shown. Dashed box indicates the area of photobleaching. Time 0 s indicates the start of recovery immediately after photobleaching. (G) Schematic representation of TRID1-WT and its PrLD deletion (Δ PrLD) mutants. (H) (Top) Phase separation of TRID1-WT (10 μ M) and TRID1- Δ PrLD (10 μ M). (Bottom) Magnified view of TRID1-WT or TRID1- Δ PrLD droplet. (I) HeLa cells expressing TRID1-WT-GFP or TRID1- Δ PrLD were treated with or without 5% 1,6-hexanediol and analyzed by fluorescence microscopy. (J) Immunofluorescent staining of 53BP1 in TRID1-GFP-expressing human embryonic kidney 293T (HEK293T) cells with or without 3 Gy IR. (K and L) HEK293T cells expressing indicated proteins were subjected to laser microirradiation and analyzed for the accumulation of DsRed-53BP1 in DSB sites by fluorescent microscopy (K). Dashed box indicates the area of laser microirradiation. The complete results are presented in fig. S27N. The relative fluorescence intensity of DsRed-53BP1 and TRID1-WT-GFP along the yellow lines was analyzed using ImageJ (L). (M) HeLa cells expressing indicated proteins were subjected to laser microirradiation and analyzed for the real-time accumulation of mCherry-Ku70 in DSB sites by fluorescence microscopy. Representative images of fluorescence are presented in fig. S27P. (N) The survival rate of control and TRID1 siRNA-soaked tardigrades with or without 500 Gy IR. At least 30 individuals were analyzed for each condition. (O) A proposed model that TRID1-mediated liquid-liquid phase separation has radioprotective effects through promoting Ku70/53BP1 recruitment to DNA damage sites and strengthening DSB repair. The data are presented as mean \pm SD [$n = 4$ replicates in (F)] or mean \pm SEM [$n = 10$ replicates in (M)]. One-way ANOVA with Tukey's post hoc test for (M). Simple survival analysis (Kaplan-Meier) with log-rank test for (N). $P > 0.05$, not significant (ns); *** $P < 0.001$; **** $P < 0.0001$. Scale bars, 10 μ m.



reporter systems (63), respectively. Expression of TRID1-WT led to a dose-dependent increase in the repair efficiency for both HR and NHEJ, whereas TRID1-ΔPrLD had a minimal effect (fig. S27, I and J). The expression of TRID1-WT and TRID1-ΔPrLD had no notable effect on cell cycle distribution (fig. S27K), suggesting that the improved repair efficiency by TRID1 was not due to alterations in the cell cycle.

To elucidate the potential mechanism underlying the enhanced DSB repair efficiency mediated by TRID1, we investigated the functional relationship between TRID1 and key factors involved in the DSB repair response. TRID1 specifically interacted with 53BP1, and this interaction was enhanced when cells were treated with x-ray irradiation (fig. S27L). Upon DNA damage, 53BP1 accumulated at damaged sites, colocalized with condensates formed by TRID1 (Fig. 3J), and TRID1 maintained higher protein levels of 53BP1 for the subsequent DNA repair (fig. S27M). Subsequently, an ultraviolet laser microirradiation system was used to generate localized DNA damage (63) to reveal the dynamic distribution between DsRed-53BP1 and GFP-TRID1. The results showed that at the DSB sites, 53BP1 was rapidly and significantly enriched in droplets formed by TRID1-WT 30 s after DNA damage, whereas in areas outside the droplets, the recruitment of 53BP1 was weak, and this difference remained very significant over time (Fig. 3, K and L, and fig. S27N). Moreover, disrupting LLPS formation of TRID1 by 1,6-hexanediol impaired the enhancement effect of recruitment of 53BP1 to DSB sites (fig. S27, N and O). In contrast, there was no difference in 53BP1 recruitment between TRID1-ΔPrLD-expressing cells and the control cells (fig. S27, N and O). These results directly indicated that TRID1-mediated LLPS enhanced the recruitment of 53BP1 to DSB sites. In addition, the accumulation of Ku70, which acts as a “tool belt” or loading protein to recruit NHEJ proteins for promoting DNA end joining (64), was also enhanced (Fig. 3M). Consistently, the survival rate of control and TRID1 siRNA-soaked tardigrades with 500 Gy x-ray irradiation was monitored. TRID1 siRNA-soaked tardigrades did not survive as well as control tardigrades after IR (Fig. 3N). All of these data suggest a scheme in which PrLD-dependent TRID1-mediated phase separation contributes to radiotolerance by enhancing DSB repair efficiency (Fig. 3O).

Non-tardigrade-specific genes also improve radiotolerance

As described in the previous section, we classified the 14,701 genes of *H. henanensis* sp. nov. into four groups and examined the role of tardigrade-specific genes in the radiotolerance. A fascinating question is whether genes in the other three groups, also known as non-tardigrade-specific genes, are involved in radiotolerance

in tardigrades. Through functional analysis, we observed distinct functional categories among the previously identified radiotolerance-related genes from the three groups (Fig. 4A). We found that up-regulated genes common to cellular organisms (I_Ce, the oldest grade) were significantly enriched in functions related to DNA replication, translation, and mitochondria (Fig. 4A). These up-regulated old proteins, which are highly conserved across evolution, play crucial roles in repairing oxidative RNA damage (65). On the other hand, up-regulated genes common to eukaryotes (II_Eu) were involved in more-complex biological processes, including proteolysis, autophagy, and NHEJ DNA repair. This group included key members of the NHEJ repair pathway, such as Rad50, Ku70, Ku80, and Artemis (data S5 and S7). For up-regulated genes common to metazoan (III_Me), we observed an overrepresentation of functions related to signal transduction. These findings suggest that different categories of the radiotolerance-related genes might contribute to the development of tardigrade radiation resistance through diverse mechanisms.

Among the radiotolerance-related genes that were not specific to tardigrades, there was an overrepresentation of mitochondrial-related genes (Fig. 4A). We calculated the average up-regulation degree [represented by the mean \log_2 fold change (\log_2 FC) values] of the up-regulated genes involved in the mitochondrial-related GO terms and found that the GO terms about MRC complex assembly were among the highest up-regulated (Fig. 4B and data S5), including genes involved in MRC complex assembly such as *BCS1*, *NDUFB8*, *NDUFB6*, *COX16*, *CIA30*, *NUBPL*, and *NDUFB4* (Fig. 4C). Among these complex assembly molecules, *BCS1* [ubiquinol-cytochrome c reductase (bc1) synthesis] and *NDUFB8* [NADH dehydrogenase (ubiquinone) 1 beta subcomplex subunit 8, mitochondrial] were specifically up-regulated in tardigrades compared with several model organisms (data S7). *BCS1* encodes a mitochondrial membrane-bound AAA (ATPases associated with diverse cellular activities) translocase, which is essential for the assembly of MRC complex III (66). Gene family expansion and contraction analysis (figs. S28 and S29, data S8, and supplementary text) revealed that the *BCS1* gene also underwent expansion in the tardigrades, with three to nine gene copies in tardigrades compared with a single gene in metazoans outside the phylum Tardigrada (Fig. 4, C and D; fig. S30A; and table S14). In the case of *H. henanensis* sp. nov., the *BCS1* duplicates were clustered and distributed at three loci on two chromosomes (fig. S30B).

The notable up-regulation of MRC complex in response to irradiation suggested a critical role for their radioprotective effect. To further validate this hypothesis, colony formation, comet, and immunofluorescence assays on

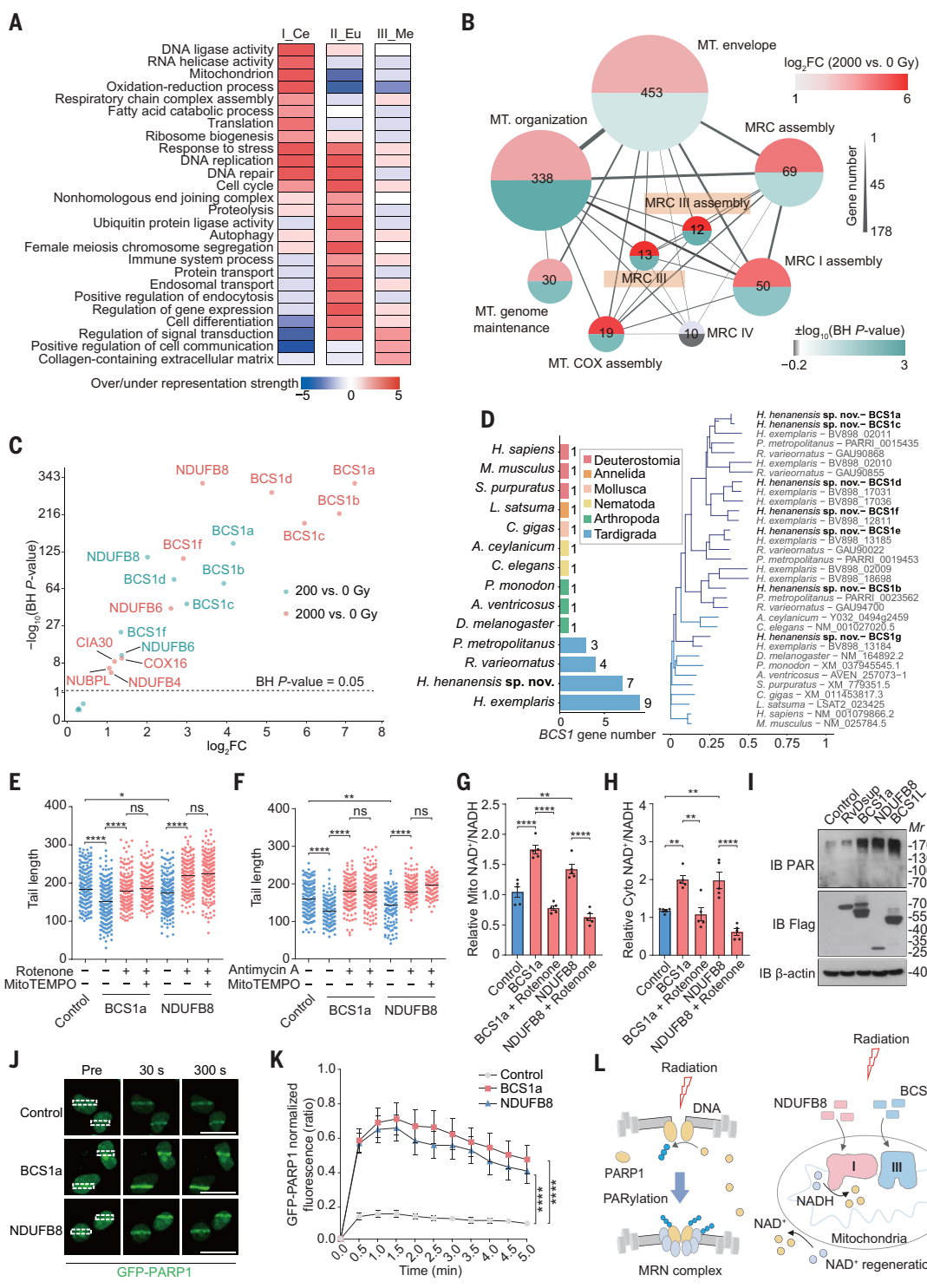
HeLa cells expressing *BCS1a* and *NDUFB8* of *H. henanensis* sp. nov. were conducted, and the results showed that *BCS1a* and *NDUFB8* enhanced cell survival and mitigated irradiation-induced DNA damage (fig. S31, A to G). *BCS1a* (a molecular chaperon for the assembly of MRC complex III) and *NDUFB8* (a component of MRC complex I) are essential for electron transfer and adenosine triphosphate (ATP) and ROS production (66, 67). Here, we found that the inhibitors of mitochondrial complexes I and III, as well as ATP synthase complex, significantly up-regulated comet length in *BCS1a* and *NDUFB8* stably expressed cells, whereas mitochondrial ROS inhibitors failed (fig. S31, H to K). Moreover, overexpression of *BCS1a* and *NDUFB8* did not change ATP and mitochondrial ROS levels, and cotreatment of the mitochondrial ROS inhibitor with mitochondrial complex I or III inhibitors also showed no significant effects on comet length when compared with mitochondrial complex I or III inhibitors groups (Fig. 4, E and F, and fig. S31, L to N). These results indicated that *BCS1a* and *NDUFB8* potentially regulated electron transfer. Subsequently, we found that *BCS1a* formed a heptamer, just like *BCS1L* (68, 69), and *NDUFB8* was assembled into mitochondrial respiratory complex I, and both *BCS1a* and *NDUFB8* increased the amount of mitochondrial respiratory super complex I_IIII₂IV₁ (SCI_IIII₂IV₁) (fig. S31, O to R). Consistently, up-regulated activities of complex I by *BCS1a* and *NDUFB8* were significantly decreased with mitochondrial complex I inhibitor (fig. S31S). Increased electron transfer caused by SCI_IIII₂IV₁ formation potentially accelerated nicotinamide adenine dinucleotide (NAD⁺) production in the mitochondria and subsequently accelerated cytosol NAD⁺ regeneration (70, 71). As expected, NAD⁺/NADH ratios in cytoplasm and mitochondria both increased in *BCS1* and *NDUFB8* overexpressed cells (Fig. 4, G and H, and fig. S31, T and U). NAD⁺, generated by the mitochondrial respiratory chain, serves as an adenosine diphosphate (ADP)-ribose donor for poly(ADP-ribosylation) (PARylation) catalyzed by poly (ADP-ribose) polymerase 1 (PARP1) in maintaining the efficiency and accuracy of DNA repair (72). Notably, up-regulated cytosol NAD⁺ regeneration provided more NAD⁺ for PARylation in *BCS1a* and *NDUFB8* overexpressed cells (Fig. 4I). This promoted the auto-PARylation of PARP1, the recruitment of PARP1 to DNA damage sites, and recruitment of DNA repair proteins MRE11, RAD50, and NBS1 (Fig. 4, J and K, and fig. S31, V and W). All the above results demonstrated that mitochondria protein *BCS1a* and *NDUFB8* exerted their anti-radiation effect through promoting NAD⁺ regeneration and PARylation (Fig. 4L).

Discussion

The capability of tardigrades to survive under the harshest conditions continues to reshape

Fig. 4. The role of non-tardigrade-specific genes in metazoans in radiation resistance illustrated by the mitochondrial respiratory chain (MRC) assembly protein BCS1 and NDUFB8.

(A) Over- or under-representation of the GO terms of unregulated non-tardigrade-specific genes. (B) The number of genes involved in mitochondrial-related GO terms and the relationship between them. The upper and lower half of these circles indicate the mean $\log_2 FC$ values and the enrichment degree of up-regulated genes, respectively. The thickness of the line indicates the number of genes shared in both terms. BH means Benjamini-Hochberg method used in multiple test correction. (C) The fold change ($\log_2 FC$ at the transcript level) and the BH adjusted P values of the radiation-induced up-regulated genes in the MRC assembly. (D) The number of BCS1 homologous genes in 14 species across metazoans and a phylogenetic tree based on protein sequence alignment. The BCS1 genes in *H. hananensis sp. nov.* are shown in bold font. The tardigrade-related branches are represented using dark-blue lines. (E) DNA fragmentations of HeLa cells stably expressing indicated proteins were assessed by tail length under 10 Gy x-ray irradiation with or without 10 μ M rotenone pretreatment for 6 hours (or cotreatment of 100 μ M mitoTEMPO for 2 hours). At least 150 cells were analyzed for each condition. (F) DNA fragmentations of HeLa cells stably expressing indicated proteins were assessed by the tail length under 10 Gy x-ray irradiation with or without 10 μ M antimycin A pretreatment for 2 hours (or cotreatment of 100 μ M mitoTEMPO for 2 hours). At least 130 cells were analyzed for each condition. (G and H) HeLa cells transfected with the indicated proteins were harvested for mitochondrial (G) and cytosol (H) NAD⁺/NADH analysis with SoNar probes. (I) Immunoblot of PARylation in HEK293T cells transfected with indicated proteins under 10 Gy IR. (J and K) HEK293T cells expressing indicated proteins were subjected to laser microirradiation and analyzed for the accumulation of GFP-PARP1 in DSB sites by fluorescent microscopy in (J). Dashed box indicates the area of laser microirradiation. Scale bars, 10 μ m. The real-time recruitment of GFP-PARP1 was analyzed in (K). (L) A proposed model that mitochondria proteins BCS1a and NDUFB8 have radioprotection effects through promoting NAD⁺ regeneration and accelerating PARP1-mediated PARylation to strengthen DSB repair. The median values are shown as a black bar in (E) and (F). The data are presented as mean \pm SEM [$n = 5$ replicates in (G) and (H) or $n = 12$ replicates in (K)]. The unit of tail length is micrometers. Kruskal-Wallis test followed by Dunn's test for (E) and (F). One-way ANOVA with Tukey's post hoc test for (G), (H), and (K). $P > 0.05$, not significant (ns); * $P < 0.05$; ** $P < 0.01$; **** $P < 0.0001$.



our concept of the limits of animal life on Earth. Our findings broaden the spectrum of possible sources of betalain pigments in nature and expand the understanding of its function beyond the plant kingdom. In metazoans, DODA is also found in the domestic silkworm (*Bombyx mori*) and other lepidopteran insects and likely horizontally transferred from plants (73), fungi (74–76), or bacteria (76). Phylogenetic analysis showed that the tardigrade DODA clade was embedded within the betalain-producing bacteria and fungi DODA clade, whereas the lepidopteran DODAs form an independent clade close to DODAs from betalain-producing plants (fig. S13, A and B). Tardigrade DODAs share no common evolutionary origin with DODAs in plant or lepidopteran insects. This betalain biosynthesis gene is widespread and has a complex evolutionary history. Colony formation assays demonstrated that HhDODA1-H16A still had little radioprotective effect (fig. S23A) at 3 Gy, indicating that HhDODA1 may have additional functions in addition to betalain synthesis. Besides DODAs, *H. henanensis* sp. nov. has 285 genes involved in antistress mechanisms (data S9), consistent with previous reports on other tardigrade species (8–10). Fifteen antioxidant response genes were up-regulated after exposure to radiation (data S9). These results suggest a multitude of independent radiation tolerance mechanisms across tardigrade species. The relationship between HGT and the resistance to the extreme environment of tardigrades remains largely unknown. Only catalase and trehalose-6-phosphate synthase (TPS) genes likely associated with anhydrobiosis in *R. varieornatus* have been reported to derive from HGT (8, 9, 14). The function of other genes identified in our study to be putatively derived from HGT and their relation to stress tolerance await further study. Fundamentally, our results highlight that integration and functional assimilation of exogenous genes represent an important driving force in tardigrade evolution.

A growing body of evidence indicates that cells adapt to stress conditions through phase separation-dependent mechanisms (62). Studies have reported that tardigrades use three families of the tardigrade-specific intrinsically disordered proteins, cytosolic abundant heat soluble (CAHS) proteins, secreted abundant heat soluble (SAHS) proteins, and mitochondrial abundant heat soluble (MAHS) proteins to improve the tolerance to desiccation, osmotic stress, and high temperatures (18, 53, 57–60). Dsup was also reported to be intrinsically disordered (7, 23, 26, 77) with a well-known radioprotective role (8, 23–29). Our study further uncovered the function of LLPS mediated by intrinsically disordered protein TRID1 in the radiation tolerance of tardigrades. Notably, there were 12 CAHS and 9 SAHS homologous genes in *H. henanensis* sp. nov., and 11 of them were

up-regulated after radiation (data S9), supporting the cross-tolerance hypothesis (6) between desiccation and radiation. Further investigations are needed to decipher the function of these intrinsically disordered proteins in the radiation tolerance of tardigrades.

Mitochondrial dysregulation has been found to be related to human health risks associated with spaceflight radiation (78). Several studies suggested that mitochondrial proteins were up-regulated to increase the synthesis of ATP for cell repair after IR and ROS release accompanied by the production of ATP resulted in the secondary damage to IR-treated cells (79, 80). Numerous studies have demonstrated the role of NAD⁺ and its related PARylation in repair responses for cellular stress and DNA damage (72). Our study showed an unexpected link between mitochondrial proteins and nuclear DNA repair, providing an optional explanation for mitochondrial dysregulation after radiation exposure. Reports have shown that BCS1 in *R. varieornatus* could also be induced with high fold change in response to UV exposure and anhydrobiosis (9, 17), suggesting that BCS1 might be general effectors in response to various types of stresses. The role of mitochondria in the stress tolerance of tardigrades would be a fascinating research direction in future.

Conclusions

Extreme environmental resistance of extremophiles such as tardigrades is a treasure trove of unexplored molecular mechanisms of stress resistance. Our work uncovers the essential role of DODA1 in the activation of an amino acid metabolism pathway (tyrosine-DOPA-betalains axis) for mitigation of ROS, elucidates tardigrade-specific TRID1-mediated phase separation in contributing to radiotolerance by enhancing DSB repair efficiency, and provides insight into participation of BCS1 and NDUFB8 in the acceleration of mitochondrial oxidative phosphorylation and NAD⁺ regeneration. Whether the radiation tolerance of other tardigrade species occurs through conserved mechanisms or is specific in the genus *Hypsibius* warrants additional study. Functional research on these radiotolerance mechanisms of tardigrades will further broaden our understanding of cellular survival under extreme conditions and may provide inspiration for promoting human health and combating diseases.

Phylogeny and species delimitation of *Hypsibius henanensis* sp. nov.

Taxonomic account

Phylum: Tardigrada Doyère, 1840

Class: Eutardigrada Richters, 1926

Order: Parachela Schuster, Nelson, Grigarick, and Christenberry, 1980

Superfamily: Hypsibioidea Pilato, 1969 (in Marley et al. 2011)

Family: Hypsibiidae Pilato, 1969

Subfamily: Hypsibiinae Pilato, 1969

Genus: *Hypsibius* Ehrenberg, 1848

Hypsibius henanensis sp. nov. Wang, Li, Yang, and Zhang

(figs. S1 and S2, tables S1 to S5, data S1, and movies S1 to S5)

Etymology: The name “*henanensis*” refers to the Henan Province, the place where the new species was collected.

Material examined: 50 animals and 12 eggs. Specimens mounted on microscope slides in Hoyer’s medium (20 animals + 12 eggs), fixed on SEM stubs (20), and processed for DNA sequencing (10).

Type locality: 33°38'56.90"N, 111°46'30.95"E, 1200 meters above sea level: Asia, China, Henan Province, the Funiu Mountain, Laojieling area. Moss from rock and rock wall, April 2018, collected by Jun Chen, Rui Bi, and Lizhi Wang.

Type repository: Holotype (Slide fns201806182) 14 paratypes and 12 eggs were deposited at Lizhi Wang’s tardigrade collection, College of Life Sciences and Food Engineering of Shaanxi Xueqian Normal University, China.

Description of holotype: Colorless. Cuticle smooth (fig. S1A). Eyes present in living animals, but prone to dissolution in Hoyer’s medium (fig. S1A). Body length, 305 µm (table S1).

Buccal apparatus of the *Hypsibius* type (fig. S1D). Buccal tube narrow, 1.7 µm in (external) diameter. Peribuccal lamellae absent, buccal tube rigid without the ventral strengthening bar. Pharynx elliptical with well-developed apophyses, two rod-shaped macroplacoids (first macroplacoid much longer than second; 2 < 1) and a small septulum (1.0 µm long), microplacoid absent (fig. S1D). The first macroplacoid anteriorly narrowed and constricted in the middle, whereas the second with a subterminal constriction (fig. S1D).

Claws of the *Hypsibius* type, with obvious accessory points on the primary branches (fig. S1, A and F). A clear septum dividing the claw into the basal and the branch portion; septum between the primary and the secondary branch less visible (fig. S1, E and G). Claws on all legs expanded at the base (fig. S1A). Cuticular bars and pseudolunulae on legs I to III absent. Anterior claws with evident pseudolunulae (fig. S1, G and H). A posterior bar on hind legs presents between the anterior and posterior claws, joined with posterior claw bases (fig. S1, G and H).

Description of the new species: Body almost transparent in smaller specimens and whitish in larger animals; transparent after fixation in Hoyer’s medium, covered with smooth cuticle under phase-contrast microscope (PCM) (fig. S1A) and scanning electron microscope (SEM) (fig. S1, B and C), with a few individuals pearly in color. Body length up to 330 µm (table S1). Eyes present in living animals, but prone to dissolution in Hoyer’s medium.

Buccal apparatus of the *Hypsibius* type (fig. S1D). Peribuccal lamellae absent. Buccal tube narrow, from 1.3 to 2.0 μm in (external) diameter, with apophyses for the insertion of the stylet muscles (AISM) in the form of a hook, without the ventral strengthening bar (fig. S1D). Stylet furcae of the *Hypsibius* type. Pharynx elliptical, with triangular apophyses, two rod-shaped macroplacoids (the first clearly longer than the second, 2 < 1) and a small triangular septulum (0.7 to 1.1 μm long; fig. S1D), but without the microplacoid. The first macroplacoid anteriorly narrowed and constricted in the middle, whereas the second with a subterminal constriction (fig. S1D).

Claws slender, of the *Hypsibius* type (fig. S1, E to H). A septum dividing the claw into the basal and the branch portion; septum between the primary and the secondary branch typically less visible. Primary branches of all claws with accessory points. Cuticular bars and pseudolunulae on legs I to III absent. Anterior claws with evident pseudolunulae (fig. S1, E to H). A posterior bar on hind legs present between the anterior and posterior claws, joined with posterior claw bases (fig. S1, G and H).

Eggs: Roundish and smooth, deposited in exuviae (four to six per clutch).

Reproduction: In the experimental setting, with 39 isolated adults of the newly identified species (originating from the isogenic population derived from a single individual), egg laying was observed in all individuals. All these eggs hatched. Thus, we conclude that *H. henanensis* sp. nov. is parthenogenetic.

Genotypic differential diagnosis: For genotyping, all four standard DNA markers (18S rRNA, 28S rRNA, ITS-2, and COI) (12) were sequenced with high quality. All markers were represented a single haplotype (table S3). Because COI and ITS-2 are suitable for the comparison between closely related species (12, 81), we used these two marker genes to calculate the pairwise *p*-distance within the genus *Hypsibius*. The *p*-distances between the tardigrade investigated in present study and haplotypes of four available *Hypsibius* species (tables S4 and S5) were as follows: COI, from 6.6% (*H. dujardini*, MG818723) to 23.7% (*H. repentinus*, MW549048), with an average distance of 17.4%; ITS-2, from 1.9% (*H. dujardini*, MG777531) to 13.0% (*H. exemplaris*, MG800336), with an average distance of 8.9%. The phylogenetic tree also showed that *H. dujardini* is the closest tardigrade to the tardigrade in the present study (fig. S2A). To further elucidate the taxonomy of *H. henanensis* sp. nov., bPTP (82), BPP (83, 84), and ASAP (85) methods were used. We performed bPTP on the basis of the COI tree, as described in previous reports (86). The ASAP analysis was based on COI alignments with default parameters. For BPP, maximum likelihood (ML) phylogenetic tree of sequences representing four markers (18S rRNA, 28S

rRNA, ITS-2, and COI) was constructed as the guide tree, COI sequences were analyzed for species delimitation. All three methods showed that *H. henanensis* sp. nov. is clearly different from other *H. dujardini* morphogroup members (fig. S2B), indicating that *H. henanensis* sp. nov. is a new species (fig. S2C).

Phenotypic differential diagnosis: The *H. dujardini* morphogroup is characterized by a smooth cuticle and two macroplacoids and septulum in the pharynx. *Hypsibius henanensis* sp. nov. is the eighth species of the *H. dujardini* morphogroup, but it can be distinguished from the other species, and it differs specifically from the following

1) *H. dujardini* by a higher *pt* (the percent ratio of the length of a given structure to the length of the buccal tube measured from the stylet sheath opening to the end of the buccal tube) of the buccal tube internal width [1.1 to 1.7 μm (5.9 to 6.8%) in *H. henanensis* sp. nov. versus 0.3 to 1.4 μm (3.2 to 5.3%) in *H. dujardini*], by a lower *pt* of primary and secondary branches (table S2) and by the morphology of the posterior cuticular bar (connected with the posterior claw base in *H. henanensis* sp. nov. versus separated from the posterior claw base in *H. dujardini*).

2) *H. exemplaris* by a shorter septulum [0.7 to 1.1 μm (3.7 to 4.4%) in *H. henanensis* sp. nov. versus 1.3 to 2.0 μm (4.9 to 7.5%) in *H. exemplaris*], by a narrower buccal tube external width [1.3 to 1.9 μm (7.0 to 7.4%) in *H. henanensis* sp. nov. versus 1.4 to 2.5 μm (7.4 to 9.4%) in *H. exemplaris*], by a lower *pt* of anterior stylet support insertion point (57.5 to 59.6% in *H. henanensis* sp. nov. versus 65.6 to 68.4% in *H. exemplaris*) and by a lower *pt* of primary and secondary branches (table S2).

3) *H. seychellensis* by a lower *pt* of the stylet support insertion point (57.5 to 59.6% in *H. henanensis* sp. nov. versus 62.3 to 63.7% in *H. seychellensis*), by a wider *pt* of external buccal tube diameter (7.0 to 7.6% in *H. henanensis* sp. nov. versus 6.3 to 6.4% in *H. seychellensis*), by a shorter *pt* of septulum (3.7 to 4.4% in *H. henanensis* sp. nov. versus 7.1 to 8.1% in *H. seychellensis*) (table S2), and the second macroplacoid shape (elongated in *H. henanensis* sp. nov. versus granular in *H. seychellensis*).

4) *H. valentinae* by a lower *pt* of the stylet support insertion point (57.5 to 59.6% in *H. henanensis* sp. nov. versus 61.3 to 62.5% in *H. valentinae*), by a lower *pt* of macroplacoid 1 (15.6 to 17.6% in *H. henanensis* sp. nov. versus 20.6 to 22.1% in *H. valentinae*), by a relatively shorter *pt* of macroplacoid 2 (11.8 to 13.4% in *H. henanensis* sp. nov. versus 15.7 to 17.0% in *H. valentinae*) and by a slightly lower *pt* of the macroplacoid row (31.7 to 35.6% in *H. henanensis* sp. nov. versus 35.9 to 44.5% in *H. valentinae*) (table S2).

5) *H. conwentzii*, *H. heardensis*, and *H. septulatus* by the absence of cuticular bars

on bases of legs I to III (bars at internal claws I to III present in *H. conwentzii*, *H. heardensis*, and *H. septulatus*).

H. henanensis sp. nov. is new to science and was identified by integrating the analyses of morphological and morphometric traits obtained through phase contrast light microscopy, scanning electron microscopy, and DNA analysis. The *H. dujardini* used to be considered a single cosmopolitan species, but it is recognized as a species with a limited geographic range within a cosmopolitan morphogroup (i.e., polyphyletic group of phenotypically similar species). The detailed phylogeny analysis further supports that *H. henanensis* sp. nov. is a new species in *H. dujardini* morphogroup.

Methods summary

A full description of the methods can be found in the supplementary materials. The supplementary materials and methods section includes descriptions of tardigrade culture, microscopy and imaging, morphometrics, genotyping, anhydrobiotic induction and recovery, radiation treatment, genome sequencing and assembly, karyotype analysis, genome annotation and synteny analysis, horizontal gene transfer analysis, transcriptomic and proteomic experiments, differential expression and functional analysis, gene age inference, protein disorder prediction, construction of plasmids, biochemical experiments, production and purification of metabolites, spectrometry and other biochemical analysis methods, phase separation and photobleaching assays, and isolation and analysis of mitochondria.

REFERENCES AND NOTES

1. R. O. Schill, Ed., *Water Bears: The Biology of Tardigrades* (Springer, 2018). doi: [10.1007/978-3-319-95702-9](https://doi.org/10.1007/978-3-319-95702-9)
2. S. J. McInnes, A. Jørgensen, Ł. Michalczyk, 20 years of Zootaxa: Tardigrada (Ecdysozoa: Panarthropoda). *Zootaxa* **4979**, 23–24 (2021). doi: [10.11646/zootaxa.4979.15](https://doi.org/10.11646/zootaxa.4979.15); pmid: [34187018](https://pubmed.ncbi.nlm.nih.gov/34187018/)
3. K. Arakawa, Examples of extreme survival: Tardigrade genomics and molecular anhydrobiology. *Annu. Rev. Anim. Biosci.* **10**, 17–37 (2022). doi: [10.1146/annurev-animal-021419-083711](https://doi.org/10.1146/annurev-animal-021419-083711); pmid: [35167318](https://pubmed.ncbi.nlm.nih.gov/35167318/)
4. K. I. Jönsson, I. Holm, H. Tassidris, Cell biology of the tardigrades: Current knowledge and perspectives. *Results Probl. Cell Differ.* **68**, 231–249 (2019). doi: [10.1007/978-3-030-23459-1_10](https://doi.org/10.1007/978-3-030-23459-1_10); pmid: [31598859](https://pubmed.ncbi.nlm.nih.gov/31598859/)
5. J. D. Hibshman, J. S. Clegg, B. Goldstein, Mechanisms of desiccation tolerance: Themes and variations in brine shrimp, roundworms, and tardigrades. *Front. Physiol.* **11**, 592016 (2020). doi: [10.3389/fphys.2020.592016](https://doi.org/10.3389/fphys.2020.592016); pmid: [33192606](https://pubmed.ncbi.nlm.nih.gov/33192606/)
6. K. I. Jönsson, Radiation tolerance in tardigrades: Current knowledge and potential applications in medicine. *Cancers* **11**, 1333 (2019). doi: [10.3390/cancers11091333](https://doi.org/10.3390/cancers11091333); pmid: [31505739](https://pubmed.ncbi.nlm.nih.gov/31505739/)
7. T. Hashimoto, T. Kunieda, DNA protection protein, a novel mechanism of radiation tolerance: Lessons from tardigrades. *Life (Basel)* **7**, 26 (2017). doi: [10.3390/life07020026](https://doi.org/10.3390/life07020026); pmid: [28617314](https://pubmed.ncbi.nlm.nih.gov/28617314/)
8. T. Hashimoto et al., Extremotolerant tardigrade genome and improved radiotolerance of human cultured cells by tardigrade-unique protein. *Nat. Commun.* **7**, 12808 (2016). doi: [10.1038/ncomms12808](https://doi.org/10.1038/ncomms12808); pmid: [27649274](https://pubmed.ncbi.nlm.nih.gov/27649274/)
9. Y. Yoshida et al., Comparative genomics of the tardigrades *Hypsibius dujardini* and *Ramazzottius varieornatus*. *PLOS Biol.* **15**, e2002266 (2017). doi: [10.1371/journal.pbio.2002266](https://doi.org/10.1371/journal.pbio.2002266); pmid: [28749982](https://pubmed.ncbi.nlm.nih.gov/28749982/)

10. Y. Murai et al., Multiomics study of a heterotardigrade, *Echiniscus testudo*, suggests the possibility of convergent evolution of abundant heat-soluble proteins in Tardigrada. *BMC Genomics* **22**, 813 (2021). doi: 10.1186/s12864-021-08131-x; pmid: 34763673
11. Y. Hara, R. Shibahara, K. Kondo, W. Abe, T. Kunieda, Parallel evolution of trehalose production machinery in anhydrobiotic animals via recurrent gene loss and horizontal transfer. *Open Biol.* **11**, 200413 (2021). doi: 10.1098/rsob.200413; pmid: 34255978
12. P. Gąsiorek, D. Stec, W. Morek, Ł. Michalczyk, An integrative redescription of *Hypsibius dujardini* (Doyère, 1840), the nominal taxon for Hypsibioidea (Tardigrada: Eutardigrada). *Zootaxa* **4415**, 45–75 (2018). doi: 10.11646/zootaxa.4415.1.2; pmid: 30313631
13. C. Hoencamp et al., 3D genomics across the tree of life reveals condensin II as a determinant of architecture type. *Science* **372**, 984–989 (2021). doi: 10.1126/science.abe2218; pmid: 34045355
14. M. Kamiları, A. Jørgensen, M. Schiøtt, N. Møbjerg, Comparative transcriptomics suggest unique molecular adaptations within tardigrade lineages. *BMC Genomics* **20**, 607 (2019). doi: 10.1186/s12864-019-5912-x; pmid: 31340759
15. B. Mali et al., Transcriptome survey of the anhydrobiotic tardigrade *Milnesium tardigradum* in comparison with *Hypsibius dujardini* and *Richtersius coronifer*. *BMC Genomics* **11**, 168 (2010). doi: 10.1186/1471-2164-11-168; pmid: 20226016
16. C. Wang, M. A. Grohme, B. Mali, R. O. Schill, M. Frohme, Towards decrypting cryptobiosis—Analyzing anhydrobiosis in the tardigrade *Milnesium tardigradum* using transcriptome sequencing. *PLOS ONE* **9**, e92663 (2014). doi: 10.1371/journal.pone.0092663; pmid: 24651535
17. Y. Yoshida et al., Time-series transcriptomic screening of factors contributing to the cross-tolerance to UV radiation and anhydrobiosis in tardigrades. *BMC Genomics* **23**, 405 (2022). doi: 10.1186/s12864-022-08642-1; pmid: 35643424
18. T. C. Boothby et al., Tardigrades use intrinsically disordered proteins to survive desiccation. *Mol. Cell* **65**, 975–984.e5 (2017). doi: 10.1016/j.molcel.2017.02.018; pmid: 28306513
19. C. M. Clark-Hachtel et al., The tardigrade *Hypsibius exemplaris* dramatically upregulates DNA repair pathway genes in response to ionizing radiation. *Curr. Biol.* **34**, 1819–1830.e6 (2024). doi: 10.1016/j.cub.2024.03.019; pmid: 38614079
20. Y. Yoshida et al., RNA sequencing data for gamma radiation response in the extremotolerant tardigrade *Ramazzottius varieornatus*. *Data Brief* **36**, 107111 (2021). doi: 10.1016/j.dib.2021.107111; pmid: 34095369
21. M. Anoud et al., Comparative transcriptomics reveal a novel tardigrade-specific DNA-binding protein induced in response to ionizing radiation. *eLife* **13**, RP92621 (2024). doi: 10.7554/eLife.92621; pmid: 38980300
22. Y. Yoshida, A. Hirayama, K. Arakawa, Transcriptome analysis of the tardigrade *Hypsibius exemplaris* exposed to the DNA-damaging agent bleomycin. *Proc. Jpn. Acad., Ser. B, Phys. Biol. Sci.* **100**, 414–428 (2024). doi: 10.2183/pjab.pjab.100.023; pmid: 38839369
23. C. Chavez, G. Cruz-Becerra, J. Fei, G. A. Kassavetis, J. T. Kadonaga, The tardigrade damage suppressor protein binds to nucleosomes and protects DNA from hydroxyl radicals. *eLife* **8**, e74682 (2019). doi: 10.7554/eLife.47682; pmid: 31571581
24. C. Ricci et al., The tardigrade damage suppressor protein modulates transcription factor and DNA repair genes in human cells treated with hydroxyl radicals and UV-C. *Biology* **10**, 970 (2021). doi: 10.3390/biology10100970; pmid: 34681069
25. E. Shaba et al., Proteomics reveals how the tardigrade damage suppressor protein teaches transfected human cells to survive UV-C stress. *Int. J. Mol. Sci.* **24**, 11463 (2023). doi: 10.3390/ijms2411463; pmid: 37511233
26. M. Zarubin et al., The tardigrade Dsup protein enhances radiosensitivity in *Drosophila melanogaster* and acts as an unspecific repressor of transcription. *iScience* **26**, 106998 (2023). doi: 10.1016/j.isci.2023.106998; pmid: 37534176
27. C. Del Casino et al., Mitigation of UV-B radiation stress in tobacco pollen by expression of the tardigrade damage suppressor protein (Dsup). *Cells* **13**, 840 (2024). doi: 10.3390/cells13100840; pmid: 38786062
28. J. Kirke, X.-L. Jin, X.-H. Zhang, Expression of a tardigrade Dsup gene enhances genome protection in plants. *Mol. Biotechnol.* **62**, 563–571 (2020). doi: 10.1007/s12033-020-00273-9; pmid: 32955680
29. N. Kasianchuk, P. Rzymski, Ł. Kaczmarek, The biomedical potential of tardigrade proteins: A review. *Biomed. Pharmacother.* **158**, 114063 (2023). doi: 10.1016/j.biopha.2022.114063; pmid: 36495665
30. J. Chen et al., Establishment of *Hypsibius dujardini* laboratory culturing system. *Military Medical Sciences* **44**, 6 (2020).
31. S. M. Soucy, J. Huang, J. P. Gogarten, Horizontal gene transfer: Building the web of life. *Nat. Rev. Genet.* **16**, 472–482 (2015). doi: 10.1038/nrg3962; pmid: 26184597
32. A. Wagner et al., Mechanisms of gene flow in archaea. *Nat. Rev. Microbiol.* **15**, 492–501 (2017). doi: 10.1038/nrmicro.2017.41; pmid: 28502981
33. B. J. Arnold, I. T. Huang, W. P. Hanage, Horizontal gene transfer and adaptive evolution in bacteria. *Nat. Rev. Microbiol.* **20**, 206–218 (2022). doi: 10.1038/s41579-021-00650-4; pmid: 3473098
34. J. Van Etten, D. Bhattacharya, Horizontal gene transfer in eukaryotes: Not if, but how much? *Trends Genet.* **36**, 915–925 (2020). doi: 10.1016/j.tig.2020.08.006; pmid: 33012528
35. F. Husnik, J. P. McCutcheon, Functional horizontal gene transfer from bacteria to eukaryotes. *Nat. Rev. Microbiol.* **16**, 67–79 (2018). doi: 10.1038/nrmicro.2017.137; pmid: 29176581
36. Y. Yoshida, R. W. Nowell, K. Arakawa, M. Blaxter, “Horizontal gene transfer in metazoa: Examples and methods” in *Horizontal Gene Transfer: Breaking Borders Between Living Kingdoms*, T. G. Villa, M. Viñas, Eds. (Springer, 2019), pp. 203–226. doi: 10.1007/978-3-030-21862-1_7
37. P. Martínez-Rodríguez, M. A. Guerrero-Rubio, P. Henarejos-Escudero, F. García-Carmona, F. Gandía-Herrero, Health-promoting potential of betalains *in vivo* and their relevance as functional ingredients: A review. *Trends Food Sci. Technol.* **122**, 66–82 (2022). doi: 10.1016/j.tifs.2022.02.020
38. M. G. Miguel, Betalains in some species of the amaranthaceae family: A review. *Antioxidants* **7**, 53 (2018). doi: 10.3390/antiox7040053; pmid: 29617324
39. F. C. Stintzing, R. Carle, Functional properties of anthocyanins and betalains in plants, food, and in human nutrition. *Trends Food Sci. Technol.* **15**, 19–38 (2004). doi: 10.1016/j.tifs.2003.07.004
40. X. Lu, Y. Wang, Z. Zhang, Radioprotective activity of betalains from red beets in mice exposed to gamma irradiation. *Eur. J. Pharmacol.* **615**, 223–227 (2009). doi: 10.1016/j.ejphar.2009.04.064; pmid: 19446548
41. J. Cho et al., Beetroot (*Beta vulgaris*) rescues mice from γ-ray irradiation by accelerating hematopoiesis and curtailing immunosuppression. *Pharm. Biol.* **55**, 306–316 (2017). doi: 10.1080/13880209.2016.1237976; pmid: 27927068
42. G. Poltakar, A. Aharoni, “La Vie en Rose”: Biosynthesis, sources, and applications of betalain pigments. *Mol. Plant* **11**, 7–22 (2018). doi: 10.1016/j.molp.2017.10.008; pmid: 29081360
43. J. P. Carreón-Hidalgo, D. C. Franco-Vásquez, D. R. Gómez-Linton, L. J. Pérez-Flores, Betalain plant sources, biosynthesis, extraction, stability enhancement methods, bioactivity, and applications. *Food Res. Int.* **151**, 110821 (2022). doi: 10.1016/j.foodres.2021.110821; pmid: 34980373
44. F. Gandía-Herrero, F. García-Carmona, Biosynthesis of betalains: Yellow and violet plant pigments. *Trends Plant Sci.* **18**, 334–343 (2013). doi: 10.1016/j.tplants.2013.01.003; pmid: 23395307
45. L. E. Contreras-Llano, M. A. Guerrero-Rubio, J. D. Lozada-Ramírez, F. García-Carmona, F. Gandía-Herrero, First betalain-producing bacteria break the exclusive presence of the pigments in the plant kingdom. *mBio* **10**, e00345–19 (2019). doi: 10.1128/mBio.00345-19; pmid: 30890610
46. L. Christinet, F. X. Burdet, M. Zaiko, U. Hinz, J. P. Zrýd, Characterization and functional identification of a novel plant 4,5-extradiol dioxygenase involved in betalain pigment biosynthesis in *Portulaca grandiflora*. *Plant Physiol.* **134**, 265–274 (2004). doi: 10.1104/pp.103.031914; pmid: 14730069
47. W. P. Roos, A. D. Thomas, B. Kaina, DNA damage and the balance between survival and death in cancer biology. *Nat. Rev. Cancer* **16**, 20–33 (2016). doi: 10.1038/nrc.2015.2; pmid: 26678314
48. M. H. Barcellos-Hoff, C. Park, E. G. Wright, Radiation and the microenvironment – tumorigenesis and therapy. *Nat. Rev. Cancer* **5**, 867–875 (2005). doi: 10.1038/nrc1735; pmid: 16327765
49. K. I. Matsumoto, M. Ueno, Y. Shoji, I. Nakanishi, Heavy-ion beam-induced reactive oxygen species and redox reactions. *Free Radic. Res.* **55**, 450–460 (2021). doi: 10.1080/10715762.2021.1899171; pmid: 33729087
50. I. Sadownka-Bartosz, G. Bartosz, Biological properties and applications of betalains. *Molecules* **26**, 2520 (2021). doi: 10.3390/molecules26092520; pmid: 33925891
51. F. Gandía-Herrero, J. Escrivano, F. García-Carmona, The role of phenolic hydroxy groups in the free radical scavenging activity of betalains. *J. Nat. Prod.* **72**, 1142–1146 (2009). doi: 10.1021/np900131r; pmid: 19456119
52. J. Escrivano, M. A. Pedreño, F. García-Carmona, R. Muñoz, Characterization of the antiradical activity of betalains from *Beta vulgaris* L. roots. *Phytochem. Anal.* **9**, 124–127 (1998). doi: 10.1002/(SICI)1099-1565(199805/06)9:3<124::AID-PCA401>3.0.CO;2-0
53. C. Hesgrave, T. C. Boothby, The biology of tardigrade disordered proteins in extreme stress tolerance. *Cell Commun. Signal.* **18**, 178 (2020). doi: 10.1186/s12964-020-00670-2; pmid: 33148259
54. Y. Yoshida, S. Tanaka, Deciphering the biological enigma—genomic evolution underlying anhydrobiosis in the phylum tardigrada and the chironomid *Polyphemus vanderplanki*. *Insects* **13**, 557 (2022). doi: 10.3390/insects13060557; pmid: 35735894
55. J. D. Hibshman, S. Carra, B. Goldstein, Tardigrade small heat shock proteins can limit desiccation-induced protein aggregation. *Commun. Biol.* **6**, 121 (2023). doi: 10.1038/s42003-023-04512-y; pmid: 36717706
56. C. Belott, B. Janis, M. A. Menze, Liquid-liquid phase separation promotes animal desiccation tolerance. *Proc. Natl. Acad. Sci. U.S.A.* **117**, 27676–27684 (2020). doi: 10.1073/pnas.2014463117; pmid: 33077592
57. K. Nguyen, S. KC, T. Gonzalez, H. Tapia, T. C. Boothby, Trehalose and tardigrade CAHS proteins work synergistically to promote desiccation tolerance. *Commun. Biol.* **5**, 1046 (2022). doi: 10.1038/s42003-022-04015-2; pmid: 36182981
58. A. Maliki et al., Intrinsically disordered tardigrade proteins self-assemble into fibrous gels in response to environmental stress. *Angew. Chem. Int. Ed.* **61**, e202109961 (2022). doi: 10.1002/anie.202109961; pmid: 34750927
59. A. Tanaka et al., Stress-dependent cell stiffening by tardigrade tolerance proteins that reversibly form a filamentous network and gel. *PLOS Biol.* **20**, e3001780 (2022). doi: 10.1371/journal.pbio.3001780; pmid: 36067153
60. M. Yagi-Utsumi et al., Desiccation-induced fibrous condensation of CAHS protein from an anhydrobiotic tardigrade. *Sci. Rep.* **11**, 21328 (2021). doi: 10.1038/s41598-021-00724-6; pmid: 34737320
61. A. Thalhammer, G. Bryant, R. Sulcipe, D. K. Hincha, Disordered cold-regulated15 proteins protect chloroplast membranes during freezing through binding and folding, but do not stabilize chloroplast enzymes *in vivo*. *Plant Physiol.* **166**, 190–201 (2014). doi: 10.1104/pp.114.245399; pmid: 25096979
62. Y. Gao, X. Li, P. Li, Y. Lin, A brief guideline for studies of phase-separated biomolecular condensates. *Nat. Chem. Biol.* **18**, 1307–1318 (2022). doi: 10.1038/s41589-022-01204-2; pmid: 36400991
63. L. Li et al., SIRT7 is a histone desuccinylase that functionally links to chromatin compaction and genome stability. *Nat. Commun.* **7**, 12235 (2016). doi: 10.1038/ncomms12235; pmid: 27436229
64. H. H. Y. Chang, N. R. Pannunzio, N. Adachi, M. R. Lieber, Non-homologous DNA end joining and alternative pathways to double-strand break repair. *Nat. Rev. Mol. Cell Biol.* **18**, 495–506 (2017). doi: 10.1038/nrm.2017.48; pmid: 28512351
65. E. J. Wurtmann, S. L. Wolin, RNA under attack: Cellular handling of RNA damage. *Crit. Rev. Biochem. Mol. Biol.* **44**, 34–49 (2009). doi: 10.1080/10409230820594043; pmid: 19089684
66. N. Wagener, M. Ackermann, S. Funès, W. Neupert, A pathway of protein translocation in mitochondria mediated by the AAA-ATPase Bcs1. *Mol. Cell* **44**, 191–202 (2011). doi: 10.1016/j.molcel.2011.07.036; pmid: 22017868
67. D. A. Stroud et al., Accessory subunits are integral for assembly and function of human mitochondrial complex I. *Nature* **538**, 123–126 (2016). doi: 10.1038/nature19754; pmid: 27263371
68. L. Kater et al., Structure of the Bcs1 AAA-ATPase suggests an airlock-like translocation mechanism for folded proteins. *Nat. Struct. Mol. Biol.* **27**, 142–149 (2020). doi: 10.1038/s41594-019-0364-1; pmid: 31988523
69. W. K. Tang et al., Structures of AAA protein translocase Bcs1 suggest translocation mechanism of a folded protein. *Nat. Struct. Mol. Biol.* **27**, 202–209 (2020). doi: 10.1038/s41594-019-0373-0; pmid: 32042153
70. I. Vercellino, L. A. Sazanov, The assembly, regulation and function of the mitochondrial respiratory chain. *Nat. Rev. Mol. Cell Biol.* **23**, 141–161 (2022). doi: 10.1038/s41580-021-00415-0; pmid: 34621061
71. M. H. Broeks et al., The malate-aspartate shuttle is important for de novo serine biosynthesis. *Cell Rep.* **42**, 113043 (2023). doi: 10.1016/j.celrep.2023.113043; pmid: 37647199

72. M. Kang, S. Park, S. H. Park, H. G. Lee, J. H. Park, A double-edged sword: The two faces of PARylation. *Int. J. Mol. Sci.* **23**, 9826 (2022). doi: [10.3390/ijms23179826](https://doi.org/10.3390/ijms23179826); pmid: [36077221](https://pubmed.ncbi.nlm.nih.gov/36077221/)
73. B. Zhu *et al.*, Horizontal gene transfer in silkworm, *Bombyx mori*. *BMC Genomics* **12**, 248 (2011). doi: [10.1186/1471-2164-12-248](https://doi.org/10.1186/1471-2164-12-248); pmid: [21595916](https://pubmed.ncbi.nlm.nih.gov/21595916/)
74. B. F. Sun *et al.*, Multiple ancient horizontal gene transfers and duplications in lepidopteran species. *Insect Mol. Biol.* **22**, 72–87 (2013). doi: [10.1111/imbo.12004](https://doi.org/10.1111/imbo.12004); pmid: [23211014](https://pubmed.ncbi.nlm.nih.gov/23211014/)
75. C. F. Wang, W. Sun, Z. Zhang, Functional characterization of the horizontally transferred 4.5-DOPA extradiol dioxygenase gene in the domestic silkworm, *Bombyx mori*. *Insect Mol. Biol.* **28**, 409–419 (2019). doi: [10.1111/imbo.12558](https://doi.org/10.1111/imbo.12558); pmid: [30537278](https://pubmed.ncbi.nlm.nih.gov/30537278/)
76. Y. Li *et al.*, HGT is widespread in insects and contributes to male courtship in lepidopterans. *Cell* **185**, 2975–2987.e10 (2022). doi: [10.1016/j.cell.2022.06.014](https://doi.org/10.1016/j.cell.2022.06.014); pmid: [35853453](https://pubmed.ncbi.nlm.nih.gov/35853453/)
77. M. Mínguez-Toral, B. Cuevas-Zúñiga, M. Garrido-Arandia, L. F. Pacios, A computational structural study on the DNA-protecting role of the tardigrade-unique Dsp protein. *Sci. Rep.* **10**, 13424 (2020). doi: [10.1038/s41598-020-70431-1](https://doi.org/10.1038/s41598-020-70431-1); pmid: [32770133](https://pubmed.ncbi.nlm.nih.gov/32770133/)
78. W. A. da Silveira *et al.*, Comprehensive multi-omics analysis reveals mitochondrial stress as a central biological hub for spaceflight impact. *Cell* **183**, 1185–1201.e20 (2020). doi: [10.1016/j.cell.2020.11.002](https://doi.org/10.1016/j.cell.2020.11.002); pmid: [33242417](https://pubmed.ncbi.nlm.nih.gov/33242417/)
79. P.-C. Fan *et al.*, Quantitative proteomics reveals mitochondrial respiratory chain as a dominant target for carbon ion radiation: Delayed reactive oxygen species generation caused DNA damage. *Free Radic. Biol. Med.* **130**, 436–445 (2019). doi: [10.1016/j.freeradbiomed.2018.10.449](https://doi.org/10.1016/j.freeradbiomed.2018.10.449); pmid: [30395972](https://pubmed.ncbi.nlm.nih.gov/30395972/)
80. T. Yamamori *et al.*, Ionizing radiation induces mitochondrial reactive oxygen species production accompanied by upregulation of mitochondrial electron transport chain function and mitochondrial content under control of the cell cycle checkpoint. *Free Radic. Biol. Med.* **53**, 260–270 (2012). doi: [10.1016/j.freeradbiomed.2012.04.033](https://doi.org/10.1016/j.freeradbiomed.2012.04.033); pmid: [22580337](https://pubmed.ncbi.nlm.nih.gov/22580337/)
81. D. Stec, R. Smolak, Ł. Kaczmarek, Ł. Michalczyk, An integrative description of *Macrobiotus paulinae* sp. nov. (Tardigrada: Eutardigrada: Macrobiotidae: *hufelandi* group) from Kenya. *Zootaxa* **4052**, 501–526 (2015). doi: [10.11164/zootaxa.4052.5.1](https://doi.org/10.11164/zootaxa.4052.5.1); pmid: [26701450](https://pubmed.ncbi.nlm.nih.gov/26701450/)
82. J. Zhang, P. Kapli, P. Pavlidis, A. Stamatakis, A general species delimitation method with applications to phylogenetic placements. *Bioinformatics* **29**, 2869–2876 (2013). doi: [10.1093/bioinformatics/btt499](https://doi.org/10.1093/bioinformatics/btt499); pmid: [23990417](https://pubmed.ncbi.nlm.nih.gov/23990417/)
83. Z. Yang, The BPP program for species tree estimation and species delimitation. *Curr. Zool.* **61**, 854–865 (2015). doi: [10.1093/czoolo/61.5.854](https://doi.org/10.1093/czoolo/61.5.854)
84. A. Luo, C. Ling, S. Y. W. Ho, C. D. Zhu, Comparison of methods for molecular species delimitation across a range of speciation scenarios. *Syst. Biol.* **67**, 830–846 (2018). doi: [10.1093/sysbio/syy011](https://doi.org/10.1093/sysbio/syy011); pmid: [29462495](https://pubmed.ncbi.nlm.nih.gov/29462495/)
85. N. Puillandre, S. Brouillet, G. Achaz, ASAP: Assemble species by automatic partitioning. *Mol. Ecol. Resour.* **21**, 609–620 (2021). doi: [10.1111/1755-0998.13281](https://doi.org/10.1111/1755-0998.13281); pmid: [33058550](https://pubmed.ncbi.nlm.nih.gov/33058550/)
86. D. Stec *et al.*, Integrative taxonomy resolves species identities within the *Macrobiotus pallarii* complex (Eutardigrada: Macrobiotidae). *Zoological Lett.* **7**, 9 (2021). doi: [10.1186/s40851-021-00176-w](https://doi.org/10.1186/s40851-021-00176-w); pmid: [34044886](https://pubmed.ncbi.nlm.nih.gov/34044886/)
87. T. Chen *et al.*, The Genome Sequence Archive Family: toward explosive data growth and diverse data types. *Genomics Proteomics Bioinformatics* **19**, 578–583 (2021). doi: [10.1016/j.gpb.2021.08.001](https://doi.org/10.1016/j.gpb.2021.08.001); pmid: [34400360](https://pubmed.ncbi.nlm.nih.gov/34400360/)
88. CNCB-NGDC Members and Partners, Database resources of the National Genomics Data Center, China National Center for Bioinformation in 2023. *Nucleic Acids Res.* **51**, D18–D28 (2023). doi: [10.1093/nar/gkac1073](https://doi.org/10.1093/nar/gkac1073); pmid: [36420893](https://pubmed.ncbi.nlm.nih.gov/36420893/)
89. M. Chen *et al.*, Genome Warehouse: A public repository housing genome-scale data. *Genomics Proteomics Bioinformatics* **19**, 584–589 (2021). doi: [10.1016/j.gpb.2021.04.001](https://doi.org/10.1016/j.gpb.2021.04.001); pmid: [34175476](https://pubmed.ncbi.nlm.nih.gov/34175476/)
90. J. Ma *et al.*, iProX: An integrated proteome resource. *Nucleic Acids Res.* **47**, D1211–D1217 (2019). doi: [10.1093/nar/gky869](https://doi.org/10.1093/nar/gky869); pmid: [30252093](https://pubmed.ncbi.nlm.nih.gov/30252093/)
91. T. Chen *et al.*, iProX in 2021: Connecting proteomics data sharing with big data. *Nucleic Acids Res.* **50**, D1522–D1527 (2022). doi: [10.1093/nar/gkab1081](https://doi.org/10.1093/nar/gkab1081); pmid: [34871441](https://pubmed.ncbi.nlm.nih.gov/34871441/)

ACKNOWLEDGMENT

We thank Y. Yoshida (Keio University, Japan) and K. Arakawa (Keio University, Japan) for technical suggestions with culturing system, M. Matsumoto (Keio University, Japan) for assistance with karyotype analysis, X.-X. Shen (Zhejiang University, China) for valuable suggestions on HGT analysis, B. Li (Capital Medical University, China) for help with NAD⁺ detection, X. Li (Hebei University, China) for useful suggestions regarding the species delimitation analysis, L. Liang (Peking University, China) for help with protein structural analysis, and W. Zhang, Y. Xie, and S. Yi [National Center for Protein Sciences Beijing (NCPSP), China] for help with mass spectrometry analysis of betalains and imaging of tardigrades. We thank members of multiple platforms of the NCPSP for their support in microscopy imaging, gel filtration, proteomic and metabolite detection, and large-scale data processing. **Funding:** This work was supported by the National Natural Science Foundation of China (82192881 to L.Z., 32270711 to D.Y., and 22193073 to Xiaoguang Lei), Beijing Nova Program (20220484230 to D.Y.), the State Key Laboratory of Proteomics (SKLP-K202004 to D.Y., SKLP-0201704 to L.W.), the Beijing National Laboratory for Molecular Sciences (BNLMS-CXX-202106 to Xiaoguang Lei), and the New Cornerstone Science Foundation through the XPLOER PRIZE (to Xiaoguang Lei). **Author contributions:** Conceptualization: L.Z., D.Y., and Lei Li. Data curation: D.Y., Lei Li, Z.G., S.L., K.Z., Yaqi Li, and Y.F. Formal analysis: D.Y., Lei Li, Z.G., S.L., K.Z., Yaqi Li, M.D., Liangwei Li, P.S., Z.Y., Y.N., A.L., F.W., and L.W. Funding acquisition: L.Z., D.Y., L.W., and Xiaoguang Lei. Investigation: Lei Li, Z.G., K.Z., Yaqi Li, K.C., Y.F., D.Y., Z.C., Y.W., J.H., Yanyan Liu, Z.S., Jun Chen, G.W., Junmiao Chen, R.L., C.L., B.C., Y.Y., F.G., M.Y., and L.W. Methodology: Lei Li, D.Y., K.Z., K.C., Xiaoguang Lei, Jun Chen, and L.W. Project administration: L.Z., D.Y., Lei Li, and L.W. Resources: L.Z., D.Y., Xiaoguang Lei, Z.C., Z.S., and L.W. Software: S.L., K.Z.,

Yaqi Li, P.S., and D.Y. Supervision: L.Z., D.Y., Lei Li, Y.F., G.F., and L.W. Validation: L.Z., D.Y., Lei Li, Z.G., S.L., Yaqi Li, and L.W. Visualization: Lei Li, Z.G., S.L., K.Z., Yaqi Li, K.C., Y.F., B.C., and L.W. Writing – original draft: Lei Li, D.Y., Z.G., S.L., K.Z., Yaqi Li, Y.F., and L.W. Writing – review & editing: Lei Li, D.Y., G.F., L.Z., I.S., Xin Liu, C.H.L., Y.F., and L.W. **Competing interests:** The authors declare that they have no competing interests. **Data and materials availability:** All data are available in the manuscript, the supplementary materials, or in publicly accessible repositories. The raw genome sequencing and RNA sequencing data reported in this paper have been submitted to the Genome Sequence Archive ([87](https://www.ncbi.nlm.nih.gov/geo/)), the National Genomics Data Center ([88](https://www.ncbi.nlm.nih.gov/geo/)), and the China National Center for Bioinformation (CNCB)/Beijing Institute of Genomics, Chinese Academy of Sciences (<https://www.cncb.ac.cn/?lang=en>) with the accession numbers CRA012677 and CRA012673, respectively. The whole genome assembly and annotation data have been deposited in the Genome Warehouse ([89](https://www.ncbi.nlm.nih.gov/geo/)) in CNCB under the accession number GWHUDUB000000000. The corresponding Bioprojects were deposited to CNCB under the following the accession numbers: PRJCA019664 (genome sequencing/assembly) and PRJCA019678 (RNA sequencing). The CDS sequences of *DODA1*, *TRIDI*, *BCS1a*, and *NDUF8* of *H. hanenensis* sp. nov. have been deposited in the GenBase in CNCB with accession numbers C_AA044688.1, C_AA044690.1, C_AA044687.1, and C_AA044689.1, respectively. DNA sequences of 18S rRNA, 28S rRNA, ITS-2, and COI of *H. hanenensis* sp. nov. were submitted to GenBank and the accession numbers are listed in Table S3. The raw proteome data and the database searching results have been deposited to the ProteomeXchange Consortium (<https://proteomecentral.proteomexchange.org/>) via the iProX partner repository ([90, 91](https://proteomecentral.proteomexchange.org/)) with the dataset identifier PXD045537. The mass spectrometry data for the metabolites have also been deposited to the ProteomeXchange Consortium via the iProX partner repository with the dataset identifier PXD050882. The samples of *H. hanenensis* sp. nov. can be provided on request along with materials transfer agreements. The uncropped Western blotting gels are shown in fig. S32. **License information:** Copyright © 2024 the authors, some rights reserved; exclusive licensee American Association for the Advancement of Science. No claim to original US government works. <https://www.science.org/about/science-licenses-journal-article-reuse>

SUPPLEMENTARY MATERIALS

science.org/doi/10.1126/science.adl0799

Materials and Methods

Supplementary Text

Figs. S1 to S32

Tables S1 to S16

References ([92–176](#))

MDAR Reproducibility Checklist

Movies S1 to S6

Data S1 to S10

Submitted 27 September 2023; accepted 5 September 2024
10.1126/science.adl0799